Astronomy & Astrophysics manuscript no. morpho˙dens˙astroph
June 24, 2009

The zCOSMOS Redshift Survey: the role of environment and stellar mass in shaping the rise of the morphology–density relation from z ∼ 1 ⋆

L. A. M. Tasca[1,2], J.-P. Kneib[1], A. Iovino[3], O. Le Fèvre[1], K. Kovač[4], M. Bolzonella[5], S. J. Lilly[4], R. G. Abraham[6], P. Cassata[1,7], O. Cucciati[1], L. Guzzo[3], L. Tresse[1], G. Zamorani[5], P. Capak[8], B. Garilli[2], M. Scodeggio[2], K. Sheth[9], D. Vergani[5], E. Zucca[5], C. M. Carollo[4], T. Contini[10], V. Mainieri[11], A. Renzini[12], S. Bardelli[5], A. Bongiorno[13], K. Caputi[4], G. Coppa[5], S. de la Torre[1,3,2], L. de Ravel[1], P. Franzetti[2], P. Kampczyk[4], C. Knobel[4], A. Koekemoer[14], F. Lamareille[10], J. -F. Le Borgne[10], V. Le Brun[1], C. Maier[4], M. Mignoli[5], R. Pello[10], Y. Peng[4], E. Perez Montero[10,15], E. Ricciardelli[16], J. D. Silverman[4], M. Tanaka[11], U. Abbas[1,17], D. Bottini[2], A. Cappi[5], A. Cimatti[18], O. Ilbert[1], A. Leauthaud[19], D. Maccagni[2], C. Marinoni[20], H. J. McCracken[21], P. Memeo[2], B. Meneux[13,22], P. Oesch[4], C. Porciani[23], L. Pozzetti[5], R. Scaramella[24], and C. Scarlata[8]

(Affiliations can be found after the references)

Received... ; accepted...

ABSTRACT

Context. For more than two decades we have known that galaxy morphological segregation is present in the Local Universe. It is important to see how this relation evolves with cosmic time.

Aims. To investigate how galaxy assembly took place with cosmic time, we explore the evolution of the morphology–density relation up to redshift z ∼ 1 using about 10000 galaxies drawn from the zCOSMOS Galaxy Redshift Survey. Taking advantage of accurate HST/ACS morphologies from the COSMOS survey, of the well–characterised zCOSMOS 3D environment, and of a large sample of galaxies with spectroscopic redshift, we want to study here the evolution of the morphology–density relation up to z ∼ 1 and its dependence on galaxy luminosity and stellar mass. The multi–wavelength coverage of the field also allows a first study of the galaxy morphological segregation dependence on colour. We further attempt to disentangle between processes that occurred early in the history of the Universe or late in the life of galaxies.

Methods. The zCOSMOS field benefits of high–resolution imaging in the F814W filter from the Advanced Camera for Survey (ACS). We use standard morphology classifiers, optimised for being robust against band–shifting and surface brightness dimming, and a new, objective, and automated method to convert morphological parameters into early, spiral, and irregular types. We use about 10000 galaxies down to I_{AB} = 22.5 with a spectroscopic sampling rate of 33% to characterise the environment of galaxies up to z ∼ 1 from the 100 kpc scales of galaxy groups up to the 100 Mpc scales of the cosmic web. The evolution of the morphology–density relation in different environments is then studied for luminosity and stellar–mass selected, volume–limited samples of galaxies. The trends are described and related to the various physical processes that could play a relevant role in the build–up of the morphology–density relation.

Results. We confirm that the morphological segregation is present up to z ∼ 1 for luminosity–selected, volume–limited samples. The behaviour of the morphology–density relation gets flatter at fixed masses expecially above $10^{10.6}$ $M_{\odot}$. We suggest the existence of a critical mass above which the physical processes governing galaxy stellar mass also determine the shaping of the galaxy more than its environment. We finally show that at a fixed morphology there is still a residual variation in galaxy colours with density.

Conclusions. The observed evolution with redshift of the morphology–density relation offers an opportunity to trace the effect of nature and nurture as a function of environment. Even though it is based mainly on a biased view, the environmental dependence of the morphological evolution for luminosity–selected, volume–limited samples seems to indicate that nurture is in play. On the other hand, the lack of evolution observed for early–type and spiral galaxies that are more massive than $10^{10.8}$ $M_{\odot}$ independents of the environment indicates that nature has imprinted these properties early in the life of these galaxies. We conclude that the relative contribution of nature and nurture in different environments strongly depends on the mass of galaxies, consistent with a downsizing scenario.

Key words. Cosmology: observations – large scale structure of Universe – Galaxies: distances and redshifts – evolution – formation – fundamental parameters – structure

1. Introduction

In the standard picture of structure formation, the so–called cold dark matter scenario, galaxies form through the cooling and collapse of baryons within dark matter haloes (e.g. White & Rees, 1978). Haloes grow in mass through mergers and infall, in a hierarchical fashion: the largest objects are formed by mergers of smaller ones. Within this general scenario, the details of galaxy formation still must be fully understood. For example, observations seem to indicate that the most massive galaxies were already fully formed at very early times (e.g. Cimatti et al. 2004), although numerical models suggest that they in fact have grown until today through the "dry" accumulation of old populations

Send offprint requests to: L.A.M. Tasca

⋆ Based on observations obtained at the European Southern Observatory (ESO) Very Large Telescope (VLT), Paranal, Chile, as part of the Large Program 175.A-0839 (the zCOSMOS Spectroscopic Redshift Survey)

from accreted galaxies (de Lucia & Blaizot, 2007). The fact that these galaxies reside in general within large-scale overdensities suggests a connection between the total halo mass and the environment (Mo & White, 1996; Lemson & Kauffmann, 1999).

Strong correlations have been found among the measurable physical properties of galaxies: the visual morphologies of the galaxies well correlate with colour, star formation rate (SFR), mass, luminosity, surface brightness and the extent to which the bulge of a galaxy dominates (Blanton et al. 2003; Roberts & Haynes, 1994); the galaxy stellar mass is closely related to its luminosity; the surface brightness of giant ellipticals correlates with their size (Kormendy, 1977); the luminosity and the rotation velocity of the disk of spiral galaxies are related by the Tully-Fisher relation (Tully & Fisher, 1977); the Fundamental Plane relates luminosity, effective radius and surface brightness for elliptical galaxies (Faber & Jackson, 1976).

Studies to date in the local universe (Kauffmann et al. 1997; Benson et al. 2000, Kauffmann et al. 2004) suggest that observables such as morphology, stellar masses, colours and star formation histories in addition to be correlated among them are also all correlated to the environment (Hogg et al. 2003; Kauffmann et al. 2003, 2004; Blanton et al. 2005a; Baldry et al. 2006). The fraction of galaxies on the red sequence depends strongly on both stellar mass and environment. In contrast, there are strong indications that galaxy stellar masses, independently of the environment, determine the colour of a galaxy (Baldry et al. 2006). The first correlation to be discovered was the one between the environment and the galaxy type. The fact that early–type galaxies are preferentially found in denser regions than late–type galaxies was first observed by Hubble (1939) and later confirmed by various studies (Oemler, 1974; Dressler, 1980).

The two major difficulties encountered in early studies were related to the use of eye–ball morphological classification and projected density estimators. Using SDSS data Goto et al. (2003) overcome these problems and performed the more exhaustive study at low redshift using a three–dimensional local galaxy density estimation, separating galaxies in four morphological types and extending the study of the morphology–density relation into the field regions. Their results confirmed the existence in the local universe of a morphological segregation and support the Postman & Geller (1984) hypothesis that the morphology–density relation presents three density ranges of particular interest or two breaks. Postman & Geller (1984) observed that below a galaxy density of ~ 5 Mpc^{-3} all population fractions show little density dependence, while above ~ 3000 galaxies Mpc^{-3} the elliptical fraction increases steeply. Additionally they connected these regions to physical mechanisms acting on different time scales upon the galaxy population.

Ram–pressure stripping (Gunn & Gott, 1972), tidal stripping (Gallagher & Ostriker, 1978; Richstone 1976), galaxy mergers and interactions (Toomre, 1977; White, 1976), galaxy harassment and galactic cannibalism (Ostriker & Tremaine, 1975; Ostriker & Hausman, 1977; Hausman & Ostriker, 1978; Tremaine, 1981) are some of the environment–dependent physical processes which have been proposed as possible drivers of the morphology–density relation. Some of them (i.e. stripping mechanisms) just act on high density peaks and none of them can by itself explain the observed trends. Initial conditions on galaxy formation could therefore play an important role too. Hence the interpretation of the morphology–density relation is not straightforward and it is still under debate whether the destiny of a galaxy is decided once its mass is assembled or whether external players related to the environment have a role, or both.

To perform similar studies at higher redshifts is more challenging due to the difficulty in estimating the two fundamental quantities needed: galaxy morphology and overdensity. A large sample of faint galaxies with spectroscopic redshift is quite difficult to obtain at high redshift, but is necessary to properly estimate the environment. Intermediate depth surveys with HST combined with ground based spectroscopy have shown that the Hubble sequence is in place at $z \sim 1$ (e.g., Lilly at al. 1995; Abraham et al. 1996; Brinchmann et al. 1998; Abraham et al. 2007). Likewise, deep observations at high resolution were difficult to achieve before the advent of the Hubble Space Telescope (HST) Advanced Camera for Survey (ACS). Another fundamental ingredient is a multi–wavelength coverage of the observed field to provide a uniform photometry to estimate galaxy spectrophotometric properties, including masses. Dressler et al. (1997) first studied the morphology–density relation for 10 clusters at $z \sim 0.5$ and found that the strength of the relation depends on the cluster concentration. On the specific case of Cl0024+16 at $z = 0.4$, Treu et al. (2003) examined the environmental influences on the properties of cluster members from the inner core to well beyond the virial radius and found that the fraction of early–type galaxies declines steeply from the cluster centre to 1 Mpc radius and more gradually thereafter, asymptoting toward the field value at the periphery. They suggest that mechanisms such as starvation or harassment, operating over timescales of several Gyr, could explain the mild trends in the morphological mix. Further studies at high–z are mainly based on groups or clusters (Nuijten et al. 2005; Postman et al. 2005; Poggianti et al. 2008) and the first relevant attempts to extend this analysis to field galaxies (Smith et al. 2005; Capak et al. 2007; Guzzo et al. 2007; Holden et al. 2007 ; van der Wel et al. 2007) all make use of local projected surface densities to estimate the environment. In parallel, the redshift and luminosity evolution of the galaxy colour–density relation up to $z \sim 1.5$ has been carefully investigated in two fundamental works (Cooper et al. 2006; Cucciati et al. 2006).

One problem in comparing the results of these studies at different redshifts is the wide range of selection methods and density estimators adopted to measure stellar masses and especially morphologies. Van der Wel et al. (2007) is the only study where an effort of homogenisation has been done by quantifying galaxy morphologies in the local universe and at higher redshifts in an internally consistent manner.

It is widely accepted that the environment galaxies inhabit should play a significant role in their formation and evolution as well as in their star formation history. A detailed understanding of the dependence of the morphological segregation as a function of mass and luminosity up to $z \sim 1$, is therefore an important step forward in the challenging astrophysical problem of understanding the formation and evolution of galaxies. The unprecedented extension of the high–resolution HST/ACS imaging coverage in the COSMOS field (Scoville et al. 2007; Koekemor et al. 2007) allow us to estimate morphologies in a robust and homogeneous way, while at the same time sampling a variety of environments over a significant redshift range. Early analyses of this unique data set were based on the use of accurate photometric redshifts to reconstruct the density field at intermediate and high densities (Guzzo et al. 2007; Capak et al. 2007), and using non–parametric techniques to estimate galaxy morphological types (Cassata et al. 2007, Abraham et al. 2007 – see discussion in the following sections). In this paper photometric redshifts are only used for the estimation of the environment combined with the unique information provided by spectroscopic information from the first 10k redshifts of the zCOSMOS survey. This new technique al-

lows us to push our environmental measurements well into the low–density regime. At the same time, we introduce a revised morphological classification extending over the whole redshift range of interest. As a result, we can study the morphology–density relation from cluster regions to sparse environments and at different redshifts, avoiding internal inconsistencies that can be caused by the use of multiple data sets.

The present work is organised as follows: we introduce the data and the way the luminosity and mass–selected, volume–limited subsamples are created in Section 2; a brief description of the environment, luminosity and stellar mass estimates as well as of the galaxy morphology computation is presented in Section 3. The implications of our results, shown in Section 4 and 5, for the general picture of galaxy formation and evolution are discussed in Section 6. Throughout this paper, unless otherwise stated, we assume a concordance cosmology with $\Omega_M = 0.25$, $\Omega_\Lambda = 0.75$ and $H_0 = 70$ kms^{-1}Mpc^{-1}. All magnitudes are quoted in the AB system.

2. The data

2.1. zCOSMOS overview

zCOSMOS (Lilly et al. 2007) is a large spectroscopic survey undertaken in the COSMOS (Scoville et al. 2007a) field using 600 hr of observation with the VIMOS spectrograph (Le Fèvre et al. 2003) on the 8 m UT3 "Melipal" of the European Southern Observatory's Very Large Telescope (ESO-VLT). VIMOS is a multi–slit imaging spectrograph that can simultaneously observe four quadrants of roughly 7×8 arcmin^2 each, separated by a cross–shaped region 2 arcmin wide. Slit masks were prepared for the four quadrants of VIMOS using the VMMPS software (Bottini et al. 2005). The zCOSMOS redshift survey consists of two parts. The brighter, lower redshift component, the so–called zCOSMOS "bright", has a pure magnitude selection at $I_{AB} < 22.5$, similar to previous surveys (e.g. Lilly et al. 1995; Le Fèvre et al. 1995, 2005) and it covers the whole 1.7 deg^2 COSMOS field observed with the Hubble Space Telescope (HST) using the Advanced Camera for Surveys (ACS). The selection criteria for the zCOSMOS–bright survey is based on F814W total magnitudes derived fron the 0.1 arcsec resolution HST images (Koekemoer et al. 2007). After applying a pure magnitude selection in the range $15 \leq I_{AB} \leq 22.5$, we are left with a parent catalogue of $\sim 40,000$ objects, the so–called 40k sample. The 40k sample, even if primarly built from HST/ACS imaging, has an additional cleaning done by comparison with i^* images obtained with MEGACAM on the 3.6 m Canada–France–Hawaii telescope. Some objects lost in ACS images because of masking of bright stars and their spikes were recovered and included with their CFHT magnitude since CFHT images are rotated by about 10 degrees with respect to the ACS ones. The higher redshift part, the zCOSMOS "deep", is a survey aiming at observing $\sim 10,000$ galaxies selected through colour–selection criteria to have $1.4 < z < 3.0$, within the central COSMOS 1 deg^2.

2.2. The 10k zCOSMOS redshift sample

For this work we use the zCOSMOS–bright survey. The very impressive deep multi–band photometry in the COSMOS field (Taniguchi et al. 2007; Capak et al. 2007) is a key component to zCOSMOS measurements of masses, absolute magnitudes and photometric redshifts, for which an accuracy of 0.023(1+z) is achieved to $I_{AB} < 22.5$ (Oesch et al. 2009, in preparation). zCOSMOS has currently observed about 50% of the brighter, magnitude limited part of the survey. This is the so–called 10k bright sample and represents the data set used in this work. The magnitude selection at $I_{AB} < 22.5$ yields redshifts in the range $0.1 < z < 1.2$. To follow the strong spectral features around 4000Å to as high redshift as possible, the medium resolution ($R \sim 600$) grism in the red (5550–9650 Å) is used. The integration time, set to 1h, allows to secure redshifts with a high success rate and with a velocity accuracy of ~ 100 km s^{-1}. Roughly 80 masks, distributed over an area of ~ 1.5 deg^2, have been already reduced using the VIPGI software (Scodeggio et al. 2005). The high reliability of the redshift estimate is assured first by an automatic determination through the EZ software (Garilli et al. 2009, in preparation) and by the reduction of each pointing done independently by scientists in two different institutes which participate in the zCOSMOS survey. A successive redshift reconciliation is finalised by the assignment of a confidence class (see Lilly et al. 2009). An additional decimal place in the class indicates the consistency between the spectroscopic and photometric redshifts. It can take the following values: 5, if the photometric redshift is consistent with the spectroscopic one within $|z_{phot} - z_{spec}| < 0.008 \times (1+z_{spec})$; 4, if z_{phot} is not available, usually for stars or quasars; 3, only used for class=9 objects, indicating that the degeneracy $[OII]\lambda 3727 - H\alpha$ is solved; and 1, if the photometric redshift is inconsistent with the spectroscopic one, i.e., $|z_{phot} - z_{spec}| > 0.008 \times (1 + z_{spec})$. In this study we consider only galaxies with a secure redshift. This choice provides a spectroscopic confirmation rate of 99% and represents approximately 85% of the whole sample. The mean sectroscopic sampling rate of the 10k bright sample is around ~ 30%, one object out of three in the parent photometric catalogue (what we called 40k sample) has a reliable redshift. The target rate of zCOSMOS objects does not depend on the size, brightness or redshift; a large fraction of stars was excluded from the spectroscopic sample according to their photometry and spectral energy distribution (SED).

Various selection criteria are applied to select a high quality spectroscopic sample to be used in the study of the evolution of the morphology–density relation. In addition to the flag selection already described, broad–line AGNs and residual stars as well as objects with problems in the photometry (less than 2%) are also removed. The requirement of morphological information does not lead to a significant additional reduction of our sample (less than ~ 3%) . The final selected sample consists of 8245 galaxies.

Table 1. Selection of volume–limited subsamples with evolving–luminosity.

Luminosity limits	z intervals
m1 = -18.5 -z	$0.2 < z < 0.5$
m2 = -19 -z	$0.2 < z < 0.5$
m3 = -19.5 -z	$0.2 < z < 0.8$
m4 = -20 -z	$0.2 < z < 0.8$
m5 = -20.5 -z	$0.2 < z < 0.8$
m6 = -21 -z	$0.2 < z < 1.0$

2.3. Evolving–luminosity and stellar mass–selected volume–limited samples

Given the flux limited selection of the zCOSMOS–bright survey we do not sample the same absolute magnitude interval at increasing redshifts. Moving towards higher redshifts, objects are selected in a progressively brighter magnitude range. We therefore defined evolving luminosity–selected, volume–limited samples in order to study the luminosity dependence of the

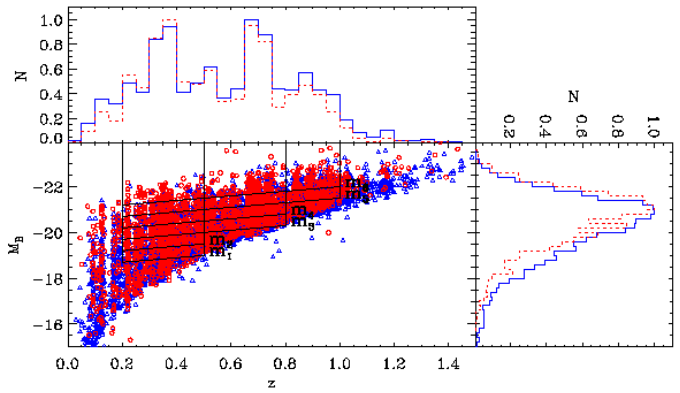

Fig. 1. Central panel: the relation between absolute B–band magnitudes and redshifts is shown as a function of the galaxy morphological type for the 10k zCOSMOS "bright" galaxy catalogue. Red empty dots represent early–type and blue empty triangles late–type galaxies. The black boxes identify the limits for the subsample selection. Top panel: normalised distribution of early (red dotted line) and late–type (blue solid line) galaxies as a function of redshift. Right panel: normalised distribution of early (red dotted line) and late–type (blue solid line) galaxies as a function of M_B absolute magnitude.

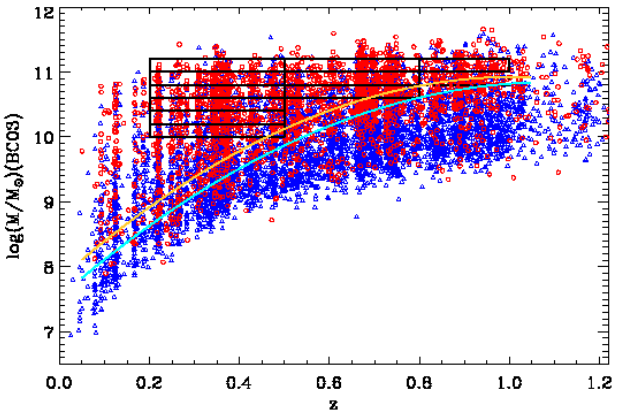

Fig. 2. Redshift distribution of galaxy stellar masses for the 10k zCOSMOS "bright" galaxy catalogue. The relation between stellar mass and redshift is shown for different galaxy morphological types. Red empty dots represent early-type and blue empty triangles late-type galaxies. The black boxes identify the limits for the subsamples selection (see text for more details). The two curves represent the adopted fit of the mass limits computed for the Bruzual & Charlot (2003) models for the early (orange line) and late (cyan solid line) galaxy population.

morphology–density relation up to z ∼ 1 being free from incompleteness. We allow for one magnitude of passive evolution between z ∼ 1 and present with the aim to select a homogeneous mix of galaxies at all redshifts, consistent with measurements in deep surveys (Lilly et al. 1996; Zucca et al. 2006). We are aware that the choice of one magnitude for the galaxy luminosity evolution is an approximate but fair correction. A more accurate value would hide our limitation in the estimation of the exact value, due to our knowledge in galaxy formation. The relation between galaxies B–band absolute magnitudes and redshifts as well as the normalised distribution of early and late–type galaxies as a function of absolute B–band magnitude and redshift are shown in Figure 1. The black boxes in the central panel of this figure identify the redshift and absolute magnitude bins chosen in our analysis in such a way that our luminosity volume–limited subsamples are not biased against a specific morphological type. The luminosity limits which assure the completeness in the considered redshift intervals are summarised in Table 1.

Likewise, when studying the mass dependence of the morphology–density relation, it is essential to assure that the subsamples used are not biased against a specific morphological type. For this purpose we define the limiting stellar mass as the mass a galaxy would have if its I–band luminosity is rescaled to the zCOSMOS selection limit $I_{lim} = 22.5$, $log(M_{lim}) = logM+0.4\times(I_{obs}-I_{lim})$ (see Pozzetti et al. 2009, for more details). As a consequence the distribution of the limiting stellar masses reflects the distribution of the stellar M/L ratio at each redshift in our sample. Different morphological types are affected in a different way by incompleteness due to the apparent magnitude selection of the survey and the scatter in the mass–luminosity relation: late–type galaxies dominate at lower masses in each redshift bin, where the completeness of early–type galaxy starts to decrease. Figure 2 presents the relation between galaxies stellar masses and redshifts for different morphological types. The overplotted black boxes represent the mass and redshift bins selection used in the analysis. Also shown are two curves, corresponding to a 95% completeness level in M/L ratio observable at the limit of the survey, which represent the fit of the limiting mass for the early and late–type population in the redshift range $0.1 < z < 1.0$ (i.e. 95% of the objects have a mass limit below this curve). These conservative selections and our direct tests make us confident that the final sample is not affected by selection effects which would bias our results and conclusions.

The use in this analysis of luminosity–selected, volume–limited samples is mainly driven by the aim of studying the luminosity dependence of the morphology–density relation and comparing, when possible, our results with previous works. Volume–limited, stellar–mass selected samples have the advantage of being a more physically motivated approach. Stellar masses are expected to evolve moderately during galaxy life, even if galaxies continuously increase in mass through merging or star formation. This is confirmed by both numerical simulations (de Lucia et al. 2006) and observational studies (Pozzetti et al. 2007). We therefore decided to use the accurate stellar mass estimation in the zCOSMOS survey to investigate the evolution of the galaxy morphological mix and its dependence on the environment for volume–limited stellar–mass selected samples. We additionally explore whether the trends which exist for luminosity volume–limited samples are still present when using stellar–mass selected, volume–limited samples.

It is important to stress, in view of the interpretation of the results shown later on, that the use of luminosity–selected, volume–limited samples or stellar–mass selected, volume–limited samples implicitly involve the study of different galaxy populations. This is clearly shown in Figure 3 where galaxy stellar masses are plotted as a function of galaxy overdensity

in three redshift intervals and for different morphological types. The galaxies plotted in the three panels correspond to the objects entering our luminosity selection, while the horizontal lines represent the mass selection. The reader should note that low mass late–type objects, in particular irregular galaxies, do not enter the mass–selected samples, since we are incomplete at these low masses, while they are included in the luminosity selected samples. A comparative study among results obtained from these two samples allows us to identify the morphological class responsible of the observed trends.

3. Data analysis

We describe in section 3.1 the new method we introduce to provide an objective and robust morphological classification of all galaxies considered for this study. We then briefly review in section 3.2 how environmental information are derived from our data and in section 3.3 how absolute magnitudes and masses are estimated. We invite the reader to refer to Kovač et al. (2009), Zucca et al. (2009), Pozzetti et al. (2009) and Cassata et al. (2009, in preparation) for a detailed overview of these measurements.

3.1. The morphological classification

Galaxy morphology is a key diagnostic of galaxy evolution. As present cosmological surveys at high redshift such as COSMOS now include more than one million of galaxies, it becomes essential to have robust tools for automatic morphological and structural classifications. A quantitative scheme should also be objective and reproducible. Motivated by these needs we developed a classification scheme based on 3 widely adopted nonparametric diagnostics of galaxies structures (Abraham et al. 2003; Lotz et al. 2004), further refining the technique applied in Cassata et al. (2007): the concentration index C, the asymmetry parameter A and the Gini coefficient G with the addition of the galaxy magnitude in the I band.

The concentration is determined using the procedure outlined in Abraham et al. (1994, 1996a) and it quantifies the central density of the galaxy light distribution. It is defined as the logarithmic ratio of the apertures containing all and 30% of the galaxy light

$$C = 5log\frac{r_{all}}{r_{30}} \quad (1)$$

The asymmetry parameter quantifies the degree of rotational symmetry of the galaxy's light distribution. It is computed by rotating each galaxy by 180° about its centre, subtracting the rotated image from the original, and dividing the sum of the absolute value of the pixels in the residual image by the sum of pixel values in the original image. A correction for background noise is also applied. Specifically A is given by

$$A = \frac{\sum_{x,y}|I_{(x,y)} - I_{180(x,y)}|}{2\sum|I_{(x,y)}|} - B_{180} \quad (2)$$

where I is the galaxy flux in pixel (x, y), I_{180} is the flux in the pixel (x, y) rotated by 180° and B_{180} is the average asymmetry of the background. Values span the range 0–1 and larger values correspond to higher intensity of the residuals;

The Gini coefficient was first introduced in Abraham et al. (2003). It provides a quantitative measure of the inequality with which galaxy's light is distributed among its constituent pixels. To first approximation it can be seen as a type of concentration index that does not rely on any underlying symmetry of the galaxy and does not require a well defined galaxy centre. Values of G span the range from 0 (if the galaxy light is uniformly distributed among galaxy's pixels) to 1 (if all the light is concentrated in few bright pixels). To be more precise, after ordering the pixels by increasing flux values, G is given by

$$G = \frac{1}{\bar{X}n(n-1)}\sum_{i=1}^{n}(2i - n - 1)X_i \quad (3)$$

where n is the number of pixels of a galaxy and $\bar{X}$ is their mean value (Glasser 1962).

To test the consistency of the measured parameters, these quantities have been computed using two independent morphological analysis codes adopting a "quasi–Petrosian" image thresholding technique (Abraham et al. 2007) and a Petrosian aperture (Lotz et al. 2004, Cassata et al. 2007). The quasi–Petrosian isophotes were introduced for the first time in Abraham et al. (2007) in order to measure galaxy properties no longer within circular apertures, whose sizes are multiple of the Petrosian radius (Petrosian 1976), but rather on isophotes adapted by an algorithm for galaxies of arbitrary shape. The quasi–Petrosian definition is therefore more suitable for measuring structural quantities of galaxies in deep high redshift surveys, considering the very diverse galaxy populations.

The next step is to convert the galactic structural parameters into morphological classes. In doing that, we improve the widely–accepted technique of subdividing the galaxy population into classes on the basis of their position in the multi–dimensional parameter space. This technique was first proposed in Abraham et al. (1996) who showed that the use of only two parameters, ie. concentration and asymmetry, was sufficient for separating galaxies among the three main morphological classes (early–type, late–type and irregulars). Subsequently other authors introduced definitions of these parameters more robust against surface–brightness selections (Brinchmann et al. 1998; Wu 1999; Bershaday et al. 2000; Conselice et al. 2000) and suggested new parameters. The idea of the CAS classification system belongs to Conselice et al. (2003) who introduced the smoothness (S). The Gini coefficient and the $M20$ moment were proposed recently by Abraham et al. (2003) and Lotz et al. (2004). In the standard approach boundaries between classes are generally plotted manually, errors are not trivial to estimate and the whole procedure lack of objectivity. Huertas-Company et al. (2008) recently proposed a generalisation of the classical non–parametric classification which uses an unlimited number of dimensions and non–linear separators, enabling for a simultaneous use of all the information brought by the different morphological parameters. We present here a new algorithm which defines the boundaries in an automated and objective way and which allows for error estimate. The main steps of the proposed methodology can be summarised as follows:

- we first measure non–parametric morphological and structural parameters for all galaxies in the sample;
- we randomly draw from the main catalogue a sample of $\sim$ 500 galaxies that we further use as a training set for the automatic classification algorithm. All galaxies in this reference sample are visually classified by at least three experts (PC, OLF, LT) to reduce misplacement and subjectivity (Naim et al. 2005). This training set is then employed to calibrate the volume filled by the data in the multi–parameter space. This critical step leads to the choice of the parameter

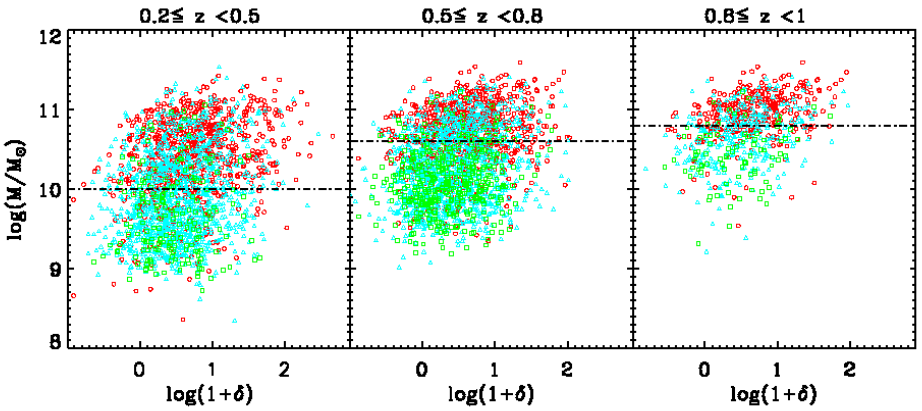

Fig. 3. Mass versus galaxy overdensity as a function of redshift. The logarithm of the stellar masses measured using the BC03 models is shown as a function of the mass–weighted galaxy overdensity computed using the 5^{th} nearest neighbour density estimator with a volume limited tracer. The relation is investigated in the three redshift intervals considered in the paper. Red empty dots represent early-type galaxies, cyan empty triangles spirals and green empty squares irregulars. The black horizontal dotted lines indicate the stellar mass limits adopted in the respective redshift bins. It appears that the great majority of irregulars and a relevant fraction of spirals are missed when applying a stellar mass selection on top of an evolving–luminosity volume–limited selection.

space regions, in which galaxies of a specific morphological type reside, that are then used for the final classification;

– we select the morphological parameters which contribute in increasing our ability to separate the various morphological classes since the information added by a specific parameter does not always turn out to be an improvement for the classification. It should be kept in mind that the simultaneous use of more parameters may complicate the interpretation of the properties of galaxies in each class. We additionally consider non–morphological parameters, such as the luminosity or the redshift of the galaxy since morphological parameters might depend on the luminosity and redshift of the galaxy (Brinchmann et al. 1998; Bershday et al. 2000). We define in this way the parameter space to be used for the automatic classification where each of the chosen parameters has a specific weight *w*, computed as the value which optimised the completeness giving the lower possible contamination;

– we compute for each galaxy (*i*) in our sample the distance d_i with respect to each galaxy in the reference sample according to the expression

$$d_i = \sum \frac{(Q_{ref} - Q_i)^2}{w_Q} \quad (4)$$

where Q it could be equal to A, C, G, S,etc... We stress that in this analysis we only use the A, C and G parameters, since they have shown to have the higher capabality to separate morphologies.
We then assign a morphological class to the galaxy depending on the most frequent class among the ones of the 11th nearest neighbours in the multi–parameter space considered;

– we finally use the algorithm to classify the visually inspected sample. The comparison of the visual and automatic classification on the control sample allows for error evaluation as well as contamination and completeness assessment.

The originality of this new galaxy's classification method mainly consists in the possibility to place galaxies in morphological classes using a multi–parameter space where the non linear boundaries are defined in an objective and reproducible way, which additionally allows for error estimate. In addition, internal parameters can be optimised to obtain a more complete or less contaminated sample relative to a specific morphological class.

The described procedure strongly depends on the quality of the imaging. It is widely recognised that image depth and the resolution are the most important ingredient needed to perform a reliable morphological classification. For the specificity of this study we benefit of the fact that the COSMOS field was imaged with the Hubble Space Telescope (HST) using the Advanced Camera for Surveys (ACS). Images were taken through the wide F814W filter and the reconstructed pixel scale is 0.03" pixel^{-1}. The full width half–maximum of the point–spread function is 0.12", yielding an unprecedented resolution of small high redshift galaxies. The median exposure depth across the field is 2028 seconds. Leautheaud et al. (2007) show that the completeness of the ACS catalogue is about 90% for objects with a FWHM of 0.2" at F814W=26.6. Taking into account the flux limited selection of the zCOSMOS survey at I=22.5 we are confident in the completeness of our sample.

More precisely, for the analysis presented in this paper, we computed non–parametric morphological parameters for all objects in the 40k catalogue starting from HST/ASC images using two independent codes. These codes differ essentially for the type of aperture used: "quasi–Petrosian" in one case and Petrosian in the other. A training sample of roughly 500 objects was drawn from the HST/ACS catalogue fulfilling the luminosity condition $18 < F814W < 24$. We performed a detailed eye–ball classification into ellipticals, lenticulars, spirals of all types (Sa, Sb, Sc, Sd), irregulars, point–like and undefined sources and we then grouped these classes into early (E,S0), spirals (Sa,Sb,Sc, Sd) and irregular types. It is this coarser classification that is considered in building the training set. We then include in the late–type class, galaxies presenting a spiral or irregular morphology. The unclassified objects are not used for the training. We then used this reference set to establish the separation regions in the multi–parameter space defined by three non–parametric quantities (concentration, asymmetry, Gini) and the galaxy's apparent magnitude. We finally run our algorithm to assign morphological classes to all objects in the 10k catalogue with the exception of objects that have entered the catalogue but were selected on CFHTLS images. The main difference we ob-

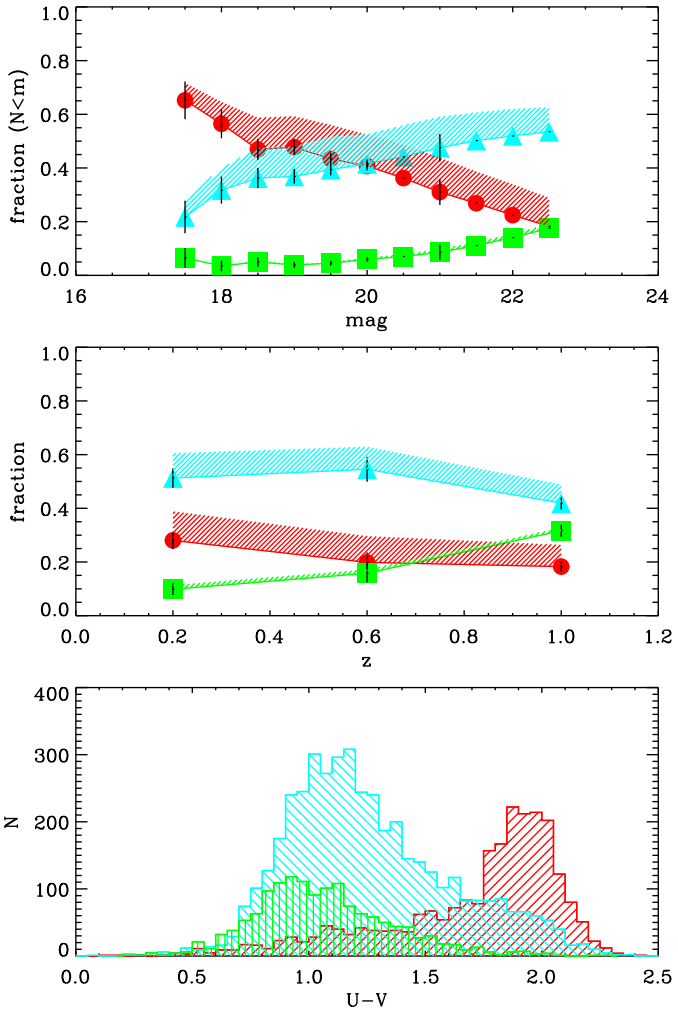

Fig. 4. Top panel: fraction of early (red filled circles), spiral (cyan filled triangles) and irregular (green filled squares) types as a function of the selection magnitude. Middle panel: fraction of early–type (red filled circles), spirals (cyan filled triangles) and irregulars (green filled squares) types as a function of redshift. In the top and middle panels the shaded regions represent the uncertainty in the morphological classification. The vertical error bars are the formal fraction errors given by simple binomial statistics. The solid lines are the interpolation obtained using the morphological classification relative to the less contaminated sample. Bottom panel: colour distribution of early–type (red 45°–inclined shaded area), spirals (cyan −45°–inclined shaded area) and irregular galaxies (green vertical shaded area).

served in the final classification is in the relative fraction of spirals and irregulars provided by the two codes. Nonetheless since for the purpose of this study spirals and irregulars are merged together in the late–type class, we are confident that our results are independent on the code used.

Figure 4 shows the general trends for the morphological catalogue used in this study. The reader should observe that the choice of clean or complete samples would change the fraction of galaxies of a specific morphological type as a function of magnitude and redshift, and should additionally be warned that this fraction is strictly related to our class definition (see Cassata et al. 2009, in preparation, for more details). The top panel shows the fraction of different morphological types as a function of I–band apparent magnitude. Three classes are considered: early–types (red filled dots), spirals (cyan filled triangles) and irregulars (green filled squares). Early–type galaxies are predominant at the brightest magnitudes, where they represent $\sim$ 65% of the whole population. Their contribution rapidly decreases, reaching $\sim$ 20% at the magnitude limit of this study. An opposite tendency is observed for the late–type population for which the fraction increases towards fainter magnitudes, where spirals are the dominant population. In the middle panel we present the evolution of the fraction of the morphological classes with redshift. We note that the sizeable growth of the fraction of irregulars above $z \sim 0.6$, balanced by the continue decrease of the elliptical fraction from $\sim$ 30% at low redshift to $\sim$ 20% at $z \sim 1$. The fraction of disk galaxies remains rather constant at $\sim$ 50%, with a mild decrease towards higher redshifts. These trends are in agreement with Conselice et al. (2004) and Cassata et al. (2005). In the first and second panels error bars are the formal fraction errors given by binomial statistics, while the uncertainty in the morphological classification is represented by the shaded areas. The shaded areas are drawn as the regions between measurements computed using visually inspected "clean" and "complete" samples. For objects in the "clean" sample (filled symbols in Figure 4) we are confident to have low contamination by other morphological types, but we know to be somewhat incomplete. Instead, the upper edge of the shaded area identifies the limit obtained with a complete but contaminated sample. A detailed explanation on how these two samples are created is given in Section 5. Nonetheless we anticipate to the reader that a pre–selection based on the galaxy SED is applied to decide on galaxies that will be further visually inspected.

The $U - V$ distribution histograms for early–type galaxies, spirals and irregulars are show in the bottom panel.

Morphological k–correction usually affects samples for which the morphological classification is performed in a single band, that maps different rest–frame wavelengths at different redshifts. In fact, the galaxy morphology varies as a function of the observed wavelength, with objects appearing morphologically later at bluer wavelengths (Windhorst et al. 2002; Papovich et al. 2003). However, since the strongest change in morphology occurs in correspondence of the Balmer break (i.e. Cassata et al. 2005; Sheth et al. 2003, 2008), the strongest bias is introduced when optical rest–frame morphologies (4000Å $< \lambda <$ 10000Å) are compared with UV ones ($\lambda <$ 4000Å). In our case, the i–band maps the rest–frame r–band at z=0.2, the V–band at z=0.6 and the B–band at z=1, therefore galaxies are observed redwards the Balmer break confidently up to z$\sim$ 0.8. Nonetheless, the effects of morphological k–correction are small when just two broad classes of early– and late–type galaxies are used (see Brinchmann et al. 1998), which is the case for a large part of the analysis carried out in this paper. Bluewards the Balmer break red elliptical galaxies, even if faint, still keep an early–type morphology. Instead spirals could be classified as irregulars since bulges are faint while bright star formation regions dominate on the disk.

3.2. The density field reconstruction

We use the density estimates of Kovač et al. (2009). The design of the zCOSMOS survey was optimised for providing an accurate reconstruction of the environments of galaxies on scales ranging from the 100 kpc to the 100 Mpc. A new algorithm (ZADE, Kovač et al. 2009) has been developed which produces

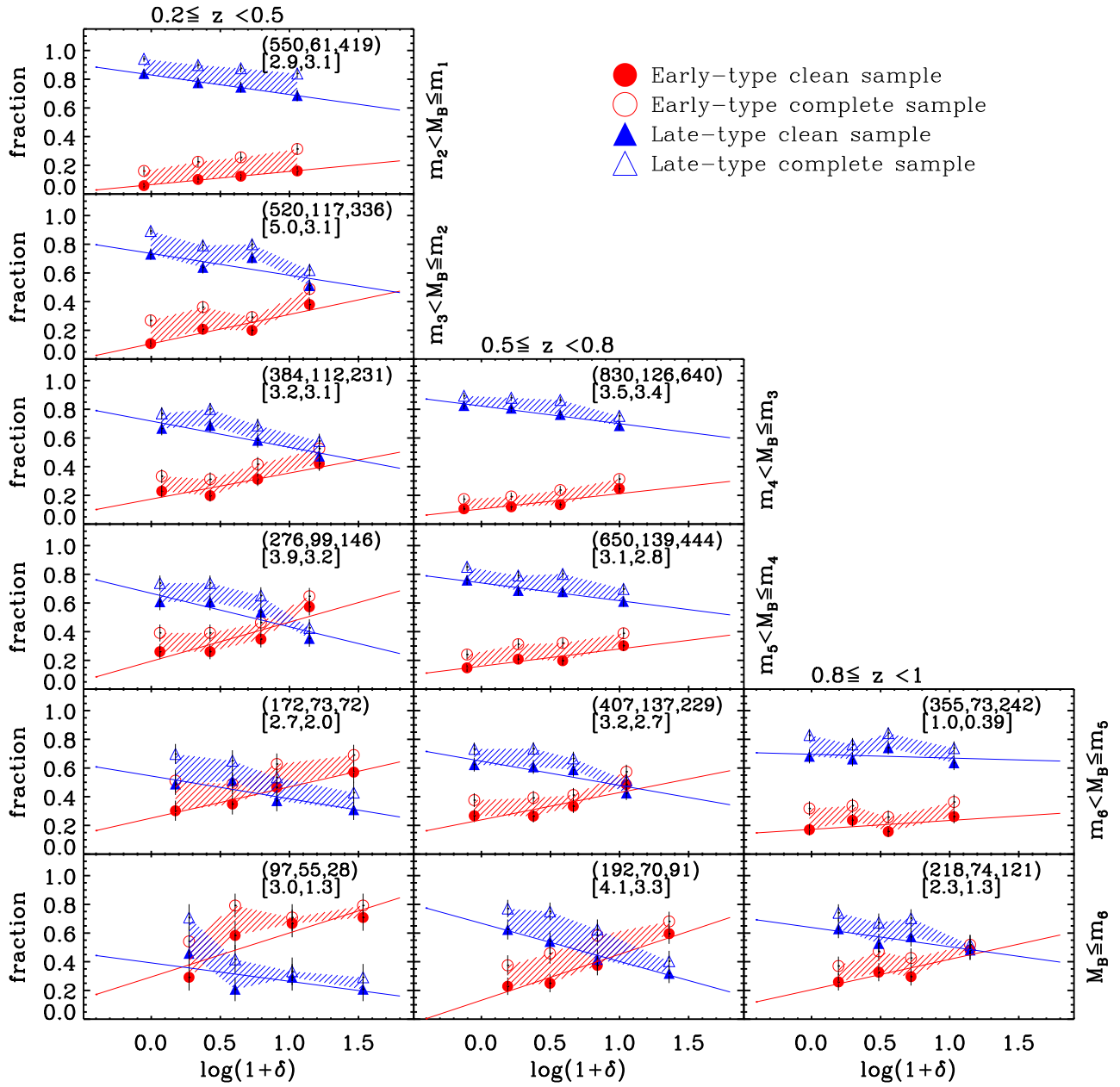

Fig. 5. Luminosity dependence of the morphology–density relation. The panels show the relation between the fraction of galaxies of different morphological types and the mass–weighted galaxy overdensity computed using the 5^{th} nearest neighbour density estimator with volume limited tracers. The morphology–density relation is presented in three redshift intervals, which increase from the left to the right of the panels (as quoted in the top), and for different absolute magnitude bins (as quoted on Table 1 and reported on the right–end side of the panels). Filled red circles and filled blue triangles represent the more conservative sample of early and late type galaxies, respectively. Empty red circles and empty blue triangles represent the more complete, but also contaminated, samples of early and late–type galaxies, respectively. All points are plotted as a function of the median overdensity in the respective quartile (see text for more details). The shaded areas represent the uncertainty in the morphological classification, while the vertical error bars are the standard fraction errors given by binomial statistics. Enclosed in parenthesis are the total number of objects in the magnitude and redshift bin considered, as well as the number of the more conservative sample of early and late–type galaxies. Within square brackets we give the significance of the deviation from zero of the slope of the linear fits relative to the clean early and late–type galaxies respectively.

environmental measurements on a broad range of scales with a noise reduction in the observed overdensities.

Cooper et al. (2005) perform numerical experiments indicating that an uncertainty smaller than 0.005 in the photometric redshift measurement together with the use of projected densities are the minimum requirements for photometric surveys to properly reconstruct the environment in all density regimes. However, in their previous investigation of the morphology–density relation with the COSMOS data, Guzzo et al. (2007) show that at the intermediate and high densities, it is in fact possible to define an unbiased estimator to succesfully benefit of the large size of photometric surveys. The innovative idea of the ZADE method adopted to reconstruct the density field used here (Kovač et al. 2009) is in fact that of combining the accuracy of spectroscopic redshift with the large number statistics of photometric redshifts. In particular, the ZADE algorithm modifies the redshift likelihood distributions, obtained from photometric redshift codes, using the information from the available spectroscopic redshifts of nearby galaxies. This is done for all the objects in the 40k catalogue not yet spectroscopically observed, in order to achieve the number statistics of photometric redshifts.

The environment reconstruction has been performed using various spatial filters with smoothing kernels of both fixed and adaptive size. The nearest neighbour technique as well as the fixed aperture with a top hat filter or Gaussian weighting methods are implemented. In particular, two samples of tracers, flux limited and volume–limited, have been considered to compute simple counts or luminosity and mass–weighted overdensities. The overdensities are finally corrected for the edge effect by dividing the measured quantity by the fraction of the area used to get the overdensity which is within the zCOSMOS survey limits. We address the reader to Kovač et al. (2009) for a complete description.

Among the abundant variety of estimators, we decided to use here the 5^{th} nearest neighbour approach with volume–limited tracers and mass–weighted overdensities. This choice allows to explore the smaller scales environments attainable by the data, while sampling the same physical scale at all redshifts, since the galaxy population used as tracer does not change with redshift. Mass–weighted overdensities are chosen since the mass is expected to be a better tracer of the environment than simple galaxy counts, since it is the galaxy stellar mass that better traces the density in a given volume. Since galaxy properties (ie. luminosity, morphology, etc.) are known to be related to the galaxy stellar mass, there is the possibility that the use of mass-weighted overdensities introduces an additional degree of correlation, in the relations with density analysed in this paper, simply because the density estimator used is itself dependent on the galaxy stellar mass. All the relations shown later on in this paper have been checked using also counts overdensities (i.e. no weight), and we are reassured by the fact that they are still present, even if sometimes at a slightly lower confidence level.

3.3. Stellar masses and absolute magnitudes estimate

Stellar masses for all galaxies in the current zCOSMOS 10k catalogue are defined as the integral of the star formation rate, subtracted by the amount of the mass of gas processed by stars and returned to the ISM during their evolution. This is estimated by fitting the galaxy spectral energy distribution, as sampled by the COSMOS multi–λ photometry, with a library of stellar population models based on Bruzual & Charlot (2003). The reader is referred to Pozzetti et al. (2007, 2009) for a full description of the methodology used to derive stellar masses and for a discussion of their robustness and intrinsic errors.

Absolute magnitudes are computed following the method described in the Appendix of Ilbert et al. (2005). The K–correction is computed using a set of templates and all the multi–band photometry data available. However, in order to reduce the template dependency, the rest frame absolute magnitude in each band is derived using the apparent magnitude from the closest observed band, shifted at the redshift of the galaxy. With this method, the applied K–correction is the smallest. For each galaxy the rest frame magnitudes were matched with the empirical set of SEDs described in Arnouts et al. (1999), composed of four observed spectra (CWW, Coleman et al. 1980) and two starburst SEDs computed with GISSEL (Bruzual & Charlot 1993). The match is performed by minimizing a χ^2 variable on these templates at the spectroscopic redshift of each galaxy.

Finally, galaxies have been divided into four spectrophotometric types based on the CWW and starburst templates (more details are given in Section 5).

4. The morphology–density relation

At present all the analyses carried out to explore the morphology–density relation confirm the Dressler et al. (1980) finding of a morphological segregation of galaxies in the local universe. This is reflected also in the widely recognised fact that at low redshift early-type galaxies are more clustered than later morphological types (e.g. Guzzo et al. 1997).

Rather than simply tracing the evolution of the morphology–density relation up to z $\sim$ 1, our goal here is to explore in detail how this evolution depends on luminosity and stellar mass. The environmental trends shown here have been tested against various ways to estimate the environment and the result shown is robust and independent of it.

4.1. Morphology–density relation: luminosity dependence

Firstly, we look whether the morphology–density relation is still present as a function of redshift up to z $\sim$ 1 and then whether there is a possible dependence of the morphology–density relation on galaxy luminosity. While it is largely accepted that galaxies with different morphologies and stellar populations preferentially reside in different environments, it has not yet been shown whether this segregation is related to the galaxy luminosity.

Using a subset of the same COSMOS imaging data used here, Guzzo et al. (2007) have shown that at z $\sim$ 0.7 the morphology-density relation depends on luminosity (cf. their Figs. 11 and 12). Here we can explore this evidence over a much broader range of redshifts and luminosities and in particular verify its role in creating the relation itself. For this pourpose we use homogeneous and complete morphology subsets of galaxies. The completeness is guaranteed by the selection of luminosity volume–limited samples, as explained in Section 2.3 and shown in Figure 1. We define luminosity volume–limited subsamples using evolving absolute magnitude cuts. We divide our main sample in three redshift bins ($0.2 \leq z < 0.5, 0.5 \leq z < 0.8$ and $0.8 \leq z < 1$) and the statistics is sufficiently high to subdivide each of them in absolute magnitude bins. The homogeneity is a consequence of the fact that galaxy morphology is measured on the HST/ACS mosaic with same method in the whole redshift range considered.

Our findings on the luminosity dependence of the morphology–density relation up to z $\sim$ 1 are shown in Figure 5.

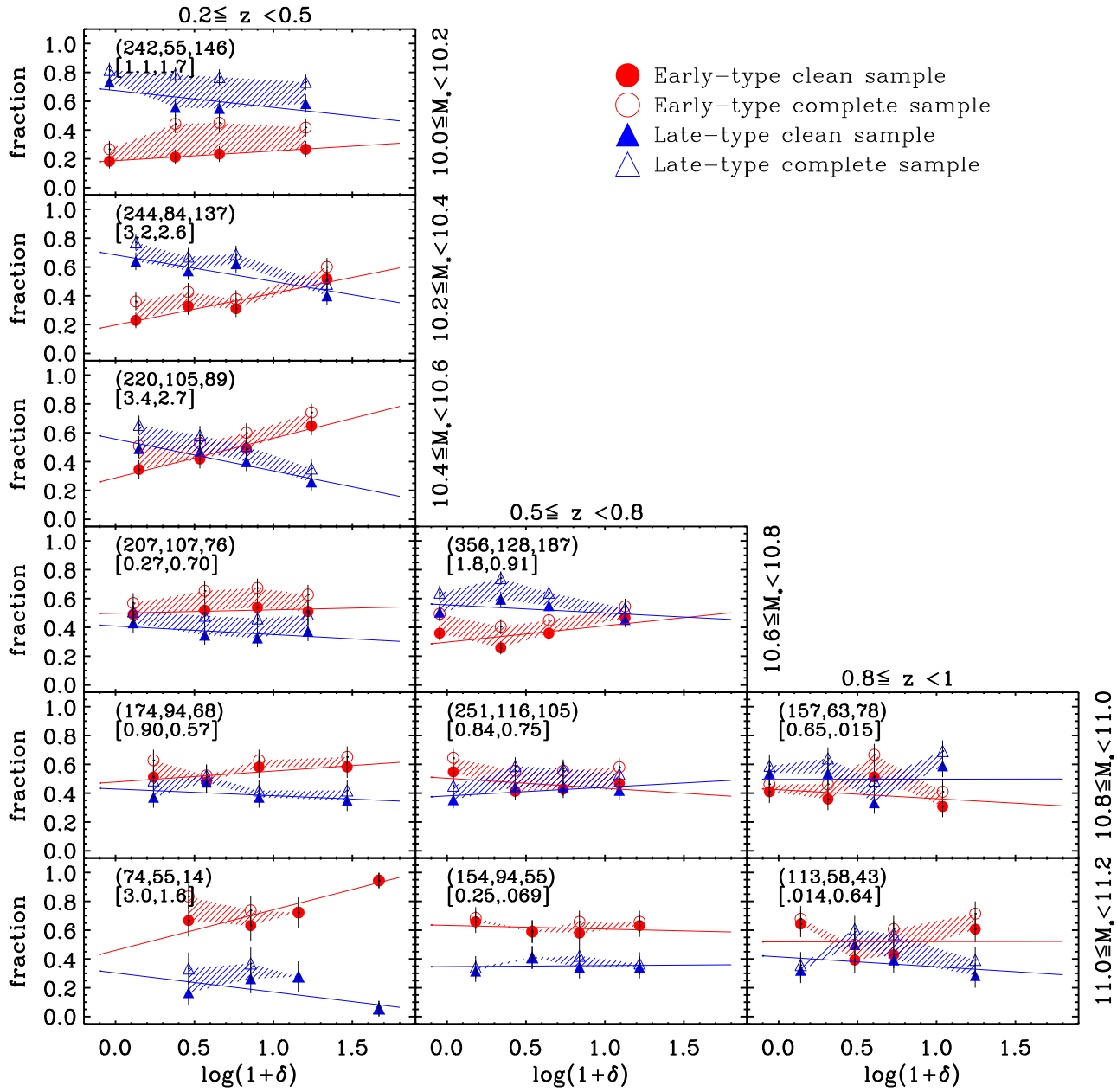

Fig. 7. Mass dependence of the morphology–density relation. The relation between the fraction of galaxies of different morphological types and the mass–weighted galaxy overdensity computed using the 5^{th} nearest neighbour density estimator with volume–limited tracers is shown in redshift and mass bins. From the left to the right the three columns correspond to higher redshifts as quoted in the label on the top. From top to bottom we consider objects of increasing mass as quoted in the label on the right–end side. Filled red circles and filled blue triangles represent the more conservative samples of early and late–type galaxies, respectively. Empty red circles and empty blue triangles represent the more complete, but also contaminated, samples of early and late–type galaxies, respectively. All points are plotted as a function of the median overdensity in the respective quartile (see text for more details). The shaded areas represent the uncertainty in the morphological classification, while the vertical error bars are the standard fraction errors given by binomial statistics. Enclosed in parenthesis are the total number of objects in the mass and redshift bin considered, as well as the number of the more conservative sample of early and late–type galaxies. Within square brackets we give the significance of the deviation from zero of the slope of the linear fits relative to the clean early and late–type galaxies, respectively.

Higher redshift bins are considered while moving to the right– end side of the plot, while luminosity is increasing from top to

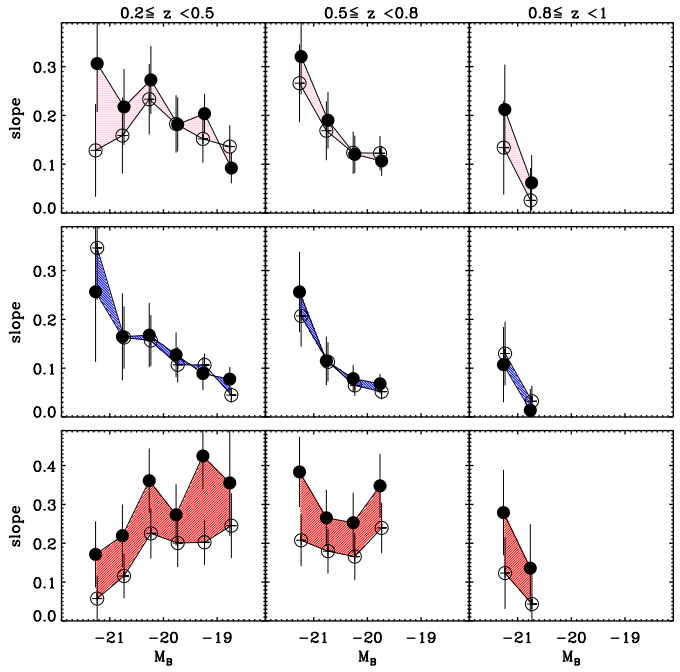

Fig. 6. Slope of the morphology-density relation as a function of galaxy luminosity, in three different redshift intervals ($0.2 \leq z < 0.5, 0.5 \leq z < 0.8$ and $0.8 \leq z < 1$). On the top row each point represents the slope of the linear fit to the morphology-density relation for early–type galaxies already shown in Figure 5. The absolute value of the slope for late–type galaxies is the same, since their behaviour with the environment is complementary to the early–type one. On the central and bottom row each point represents the slope of the linear fit to the morphology–density relation derived when the fraction of galaxies (late–type in the middle row, early–type in the bottom row) is plotted instead in logarithmic scale. The use of a logarithmic scale allows the direct visualisation of fractional changes in the abundance of a population as a function of environment, irrespective of its global abundance. In all panels filled circles correspond to the clean samples and empty circles to the complete samples. The shaded areas quantify the uncertainty due to the morphological classification.

bottom. On each panel galaxies are divided into four equally populated density bins and the median value of the density in each interval is plotted. Results are shown for the two samples discussed in Section 3.1: filled symbols refer to the more conservative and clean samples, while empty symbols are used for the complete and more contaminated ones. The shaded regions quantify the uncertainty in the morphological classification.

Fixing the redshift, i.e. looking at Figure 5 vertically, we observe a clear morphology–luminosity dependence, with a clear increase with luminosity of the fraction of early–type galaxies relative to the fraction of the later population. Spiral and irregular galaxies (grouped in the late–type population, blue triangles) are dominant at fainter absolute magnitudes and in general more abundant than ellipticals. Also we observe that the relation between the morphology of a galaxy and the environment tends to flatten out towards fainter magnitudes suggesting that brighter galaxies, at a fixed redshift, are the ones for which the morphological segregation is stronger.

Since we use evolving absolute magnitudes to define our volume–limited subsamples, Figure 5 can be read horizontally to test how the morphology–density relation evolves for a galaxy population with the same luminosity. We consider now the luminosity at which the morphology–density relation, at a fixed redshift, flattens. We observe that for higher redshift galaxies the luminosity at which galaxies of a given morphological type have the same probability to live in an overdense or underdense region is brighter with respect to low redshift galaxies. We finally point out that for galaxies with the same evolving liminosity the morphology–density relation is clearly present at low redshift, tends to flatten at intermediate redshift and almost disappears at high redshift. All the described relations are seen for both the clean and the complete samples, even if we observe that the significance of the described relations results to be higher for the clean early–type and the corresponding complete late–type samples.

The use of a logarithmic scale allows the direct visualisation of fractional changes in the abundance of a population as a function of environment, irrespective of its global abundance. For this reason, even if we do not show the equivalent of Figure 5 in logarithmic scale, we summarise in Figure 6 the main results obtained by fitting the morphology–density relation with linear and logarithmic scales. This figure shows the slope of the morphology–density ralation as a function of galaxy luminosity, in three different redshift intervals ($0.2 \leq z < 0.5, 0.5 \leq z < 0.8$ and $0.8 \leq z < 1$). In the top row each point represents the slope of the linear fit to the morphology–density relation for early–type galaxies, as already shown in Figure 5. The absolute value of the slope for late–type galaxies is not shown since it does not differ, because their behaviour with the environment is complementary to the early–type one. This is not the case in logarithmic scale. We therefore represent on the central and bottom row the slope of the linear fit to the morphology–density relation derived when the fraction of galaxies (late–type in the middle row, early–type in the bottom row) is plotted in logarithmic scale.

In the upper row of Figure 6 we plot the aforementioned slopes, in the case of a linear scale, as a function of galaxies absolute magnitude and we observe a decrement in the slope at fainter absolute magnitudes at all redshifts. We show this trend for early–type galaxies only, since as said above, the late–type population behaves in the same way. The only difference is in the inversion of the points representing the clean (filled circles) and the complete (empty circles) populations. The second row of Figure 6 shows the relation with the absolute magnitude of the slopes obtained from the linear fit of the morphology–density relation in logarithmic scale for late–type galaxies. For these galaxies the environment acts more strongly on the brightest objects at all redshifts. The three panels of the third row show the same relation as in the second row, but for early–type galaxies. We note that in the redshift interval $0.2 \leq z < 0.5$ there is an inversion of the slope behaviour as a function of luminosity with respect to the trend observed for the linear scale: the slope gets steeper towards faint luminosities. This is also the redshift–luminosity bin where the fraction of late–type galaxies is the highest (60 – 80%). As a consequence, a small fractional change in the abundance of late–type galaxies as a function of environment, is enough to steepen the logarithmic slope of the early–type galaxies. Because of the strong uncertainty in the slope estimation, the statistical significance of the shown trends is not very high, but we clearly see hints for a trend that we plan to explore with higher statistics using the zCOSMOS 20k bright sample.

We finally want to stress that while we present our results using density contrasts estimated for the smallest scale allowed by the survey design, we performed the same analysis using also

larger scale lengths to look for a specific scale that might affect galaxy properties more than others. This aspect is thoroughly examined in Cucciati et al. (2009). For the purpose of this paper it is enough to mention that the morphology–density relation survived mostly unchanged when using overdensity estimators on larger scales. The only difference is seen for the highest density quartiles in the direction of an enhanced effect when using the smallest scale, corresponding here to the 5^{th} nearest neighbour. By using this estimator we probe the densest region of groups where the morphology–density relation is expected to be stronger.

4.2. Morphology–density relation: mass dependence

Galaxies show a significant B–band rest–frame luminosity evolution between redshift zero and one, which has been shown to be dependent on the spectral (Zucca et al. 2007) and morphological (Zucca et al. 2009) types. In addition, due to bursts of star formation, the B–band rest–frame luminosity can strongly change during galaxy life.

In literature it is often claimed that galaxy stellar mass varies much less during galaxies life and can be considered as a more stable quantity to characterise a galaxy than its B–band rest–frame luminosity. Bolzanella et al. (2009) show that the galaxy stellar mass function depends on the environment. The strong variation of mass–to–light with stellar population age, and thus with the star formation history of a galaxy, together with the galaxy mass segregation produces a range of masses in a luminosity limited sample. Stellar mass should therefore represent a more physically motivated parameter on the basis of which to select galaxies, to better understand the evolution of galaxies populations.

We investigate in this Section whether the strong relations that galaxy morphologies have with the environment in luminosity–selected volume–limited samples are still present when using stellar–mass volume limited samples. This approach allows us to tackle the issue of whether the aforementioned effects are simply due to a biased view induced by the luminosity selection or a more fundamental relation among galaxy stellar mass, environment and morphology does exists. In other words, we will try to answer to the following question: are the physical processes which determine the mass more important than the environment in shaping galaxy morphology?

For this analysis we use volume–limited stellar–mass complete galaxy subsamples as explained in section 2.3 and shown in Figure 2. The main sample is divided in three redshift bins (the same used for the study of the luminosity dependence) that we now subdivide in mass bins sufficiently narrow not to mix effects related to the mass, while still having a significant statistics.

Figure 7 shows our results on the mass dependence of the morphology–density relation. As in Figure 5, the redshift increases from the left to the right panels, while stellar masses increase from top to bottom. In each panel densities have been divided into equally populated quartiles and the median value of the density in each interval is plotted. Filled and empty symbols in the various panels correspond respectively to the clean and complete samples defined in Section 3.1. The significance of the deviation from zero of the slope of the linear fit of the morphology–density relation is indicated inside the square brackets in each panel of Figure 7 for the clean early and late–type samples respectively. We observe that for all the redshift and stellar mass bins considered the significance of the slope of the fit does not depend on the sample used to compute it: a relation which is significant at more than $2-3\sigma$ with the complete sample stays significant with the clean one.

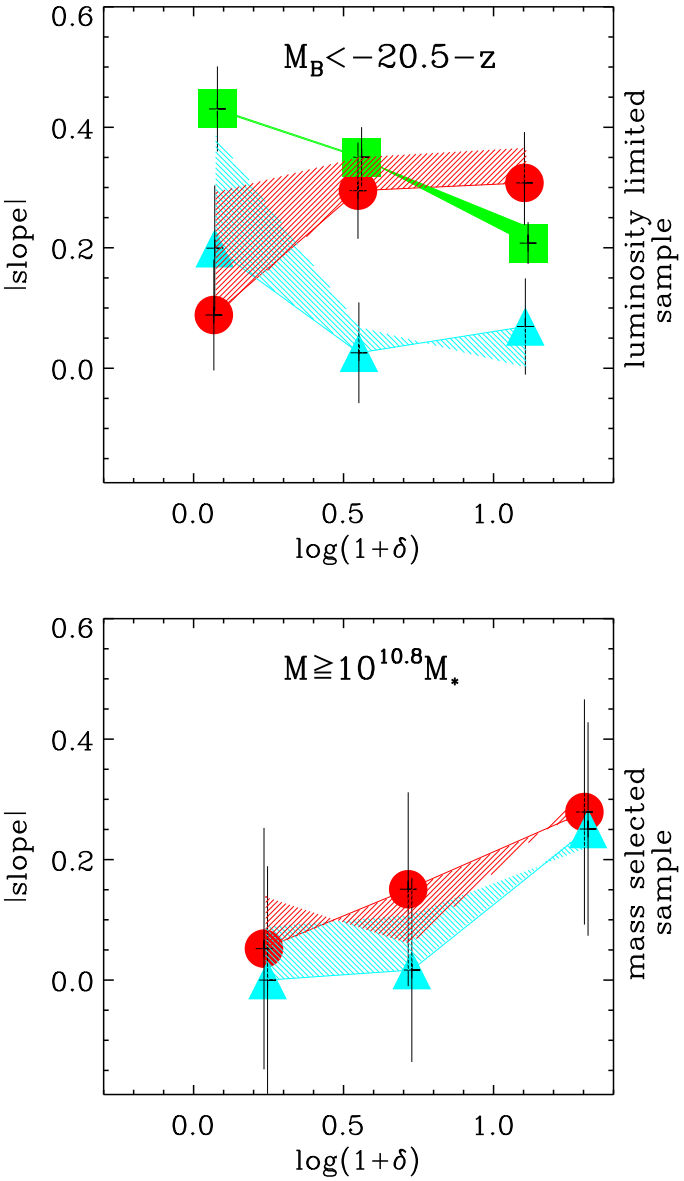

Fig. 9. The best fit slope of the fraction of early (red filled circles), spiral (cyan filled triangles) and irregular (green filled squares) population as a function of redshift, and its associated 1σ error bar, is shown as a function of the same three overdensity bins of Fig. 8. The shaded areas quantify the uncertainty in the morphological classification. The upper and bottom panels correspond respectively to the best fit slope for a luminosity–selected, volume–limited sample of galaxies with $M_B < -20.5 - z$ and a volume–limited, stellar–mass selected sample of galaxies with masses $\geq 10^{10.8} M_\odot$. The trend relative to irregular galaxies in the mass–selected sample is not shown due to the small number of irregular objects with such a high mass.

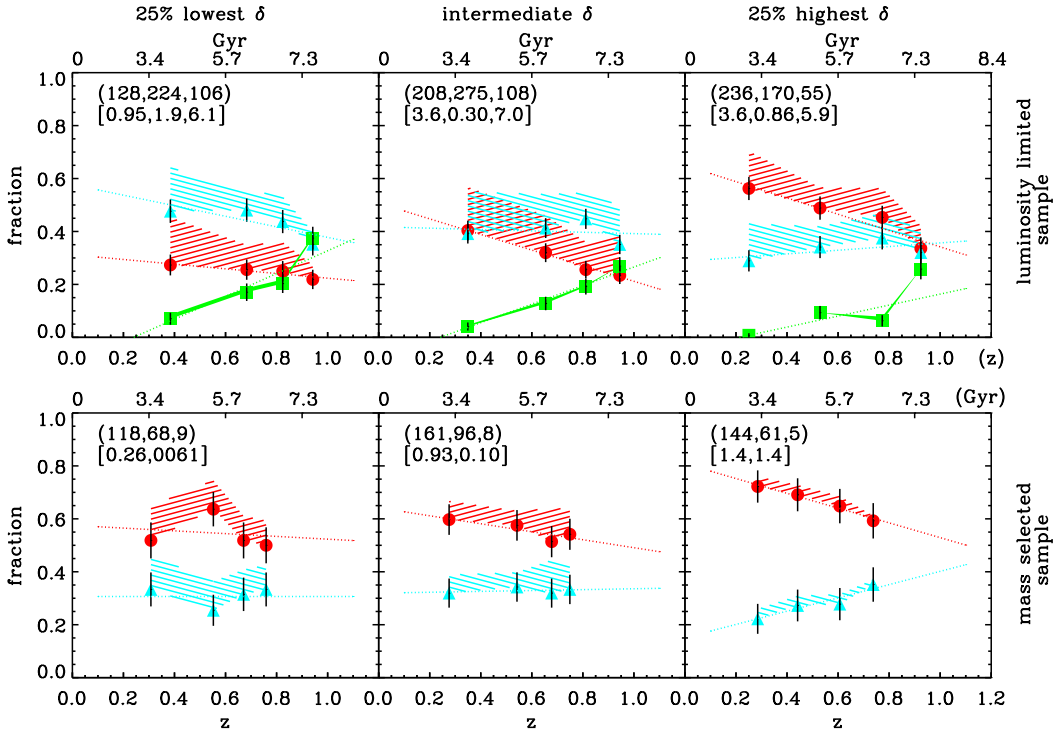

Fig. 8. Redshift evolution of the morphological fraction of galaxies as a function of the environment. In the attempt to follow the evolution of the same galaxy population, an evolving–luminosity volume limited sample of galaxies with $M_B < -20.5 - z$ is used in the top three panels, while a volume–limited, stellar–mass selected sample of galaxies with masses $\geq 10^{10.8} M_{\odot}$ is used on the three bottom panels (see text for more details). From the left to the right we explore environments of increasing density. In each panel the filled red circles represent early–type population, the filled cyan triangles spiral galaxies and the filled green squares irregular objects. The shaded regions represent the uncertainty in the morphological classification while vertical error bars are the standard fraction errors given by binomial statistics. The linear fits of the morphological fraction of galaxy types as a function of redshift for the more conservative samples are shown by the dotted lines. Enclosed in parenthesis are the total number of early–type, spiral and irregular galaxies in the considered environment. Within square brackets we give the significance of the deviation from zero of the slope of the linear fits for the three galaxy populations studied. The evolution of irregular galaxies for the mass–selected sample has not been shown due to the small number of these galaxies present in these bins.

We find that for galaxy stellar masses $\gtrsim 10^{10.8}$ M$_{\odot}$ the probability of a specific morphological type to reside in a low or high density environment is approximately the same. Expressed differently, the morphology–density relation substantially weakens at intermediate/high masses. The only possible exception is for the highest mass bin at low redshift (lower left panel) where a possible dependence of galaxy morphology on the environment appears to be present. Nonetheless we note that also this morphological trend with respect to the environment would be flat if we do not consider the last quartile corresponding to the densest environment. We assume that we are dealing with a residual relation and we explore whether the reason is the contamination of the early–type population by late–type galaxies and/or the incompleteness of late–type galaxies. In this panel the morphology–density relation is significant at 3σ for the clean sample of early–type galaxies (or complete sample of late–type) and is mostly consistent with being flat for the complete sample of early–type (or clean sample of late–type) objects. We conclude that subsequent studies with higher statistics are needed to confirm the behaviour of the morphology–density relation for very massive galaxies at low redshift.

At stellar masses smaller than $\sim 10^{10.6}$ M$_{\odot}$, which are probed by our mass–complete sample only in the first redshift bin, the fraction of early–type galaxies increases towards denser regions, while the late–type galaxies are more abundant in a sparse environment than in denser regions. The low significance of the morphology–density relation in the upper–left panel, corresponding to the lowest stellar masses and redshifts considered in this analysis, can be interpreted in at least two different ways. It could be due to the presence, in this mass and redshift interval, of a small degree of incompleteness which acts in the direction of a flattening of the relation but it could also be a real effect indicating that at low mass the role of the environment becomes again secondary with respect to the mass. If confirmed, this would support the hypothesis that there is a restricted range of stellar masses for which galaxy morphology has an environmental dependence. Since at stellar masses lower than $\sim 10^{10.0}$ M$_{\odot}$ we quickly become incomplete we conservatively conclude that the morphology–density relation does not vanish for low mass galaxies and that the inversion of behaviour we witness, with respect to higher stellar mass objects, could be seen as an indication of the existence of a critical mass which separates galaxies into two distinct families, in the framework of what already shown at low redshift by Kauffmann et al. (2003).

Finally reading the plot horizontally, approximatively equivalent to following the evolution in time of the morphological properties of galaxies with a given mass (de Lucia et al. 2006; Pozzetti et al. 2007), we qualitatively observe the evolution with redshift of the galaxy morphological types, for galaxies with the same mass. We witness a progressive increase with cosmic time

of the fraction of early–type galaxies in the same mass bin. This can be seen as the consequence of the transformation from late to early–type galaxies. The redshift evolution for very massive galaxies, the only ones for which we are complete up to z=1, is then quantitatively described in the bottom panels of Figure 8, that we fully describe in the following Section.

The main scenario resulting from our analysis is already well–drawn from our combined study of the morphology–density relation for luminosity and stellar–mass selected, volume–limited samples. The morphology–density relation is present out to z $\sim$ 1 at fixed luminosity, but its behaviour gets flatter when we look at it at fixed masses expecially above $10^{10.6}$ $M_{\odot}$. This is a clear indication that at least above $10^{10.6}$ $M_{\odot}$ the role of stellar mass is dominant with respect to the environment in determining galaxy morphology. We now want to discuss how the observed differences in the morphological segregation as a function of luminosity and stellar mass can be explained. We discuss two possible explanations which can be seen as extreme cases:

- it is a fact that for galaxies less massive than $10^{10.6}$ $M_{\odot}$ the morphology–density relation exists. If we suppose that the galaxy stellar mass function is the same in all environments then, for the lower M/L objects, a given luminosity bin could reach down to these lower mass bins. As a consequence, because of the mixing of masses, we see a residual morphology–density relation at fixed luminosity;
- Bolzonella et al. (2009) show that the galaxy stellar mass function varies with the environment with more low mass galaxies being present in low density environment. Even if the morphology–density relation were flat for all masses, which is not what we observe but can be taken as an extreme case, more low mass galaxies (most of them spirals) in low density regions than in high density ones would enter any given luminosity bin. The final effect would be that of producing a morphology–density relation at fixed luminosity. The existence of a mass segregation, such that more massive galaxies with older stellar population, which mainly have early–type morphologies, preferentially reside in denser regions, together with the strong relation of morphology, colour and M/L to mass may be the main driver in producing the observed morphology–density relation.

Even if both scenarios might partly contribute to the observed effect, we consider the second hypothesis as the more important, since the variation with the environment in the global galaxy stellar mass function (Bolzonella et al. 2009), coupled with the strong correlation between morphology and mass, appears to be large enough to produce the observed effects. In addition the first hypothesis presented is a "mixing effect", mixing together equal numbers of high and low mass objects in all environments and averaging out their individual morphology–density relations. While we claim that there is an effect below $10^{10.6}$ $M_{\odot}$, we are not overwhelmed by the strength of the morphology–density relation, at fixed mass, in this regime. Averaging it out, as mentioned above, it is just going to make it weaker still. On the other hand our second hypothesis does not even need a variation at all. The variation of the galaxy stellar mass function seems large enough over the range of ten or so needed in mass to produce the observed effect, when coupled with the strong dependence on morphology with mass.

4.3. Evolution of the morphology–density relation

The understanding of the role of the environment in the determination of the morphological mix of galaxies observed at various redshifts is fundamental for our comprehension of galaxy formation and evolution. We analyse in this section the evolution of the morphological mix of galaxies as a function of the environment for luminosity and stellar–mass selected, volume limited samples. In Section 4.2 we have shown that the morphology–density relation observed in luminosity–selected, volume–limited samples can be due to the biased view imposed by the B–band luminosity selection. The observed trends are mainly due to the fact that luminosity–selected samples include the low mass, bright blue galaxies, while they miss the equally low mass, red counterparts. Being aware that more physically motivated results come from the use of stellar–mass selected, volume–limited samples, we still consider in the following analysis both luminosity and stellar–mass selected, volume limited samples, mainly to allow the comparison to previous studies.

When looking at the observed fraction of bright galaxies of each morphological type as a function of redshift (i.e. Zucca et al., 2009), we observe that the bright late–type population becomes increasingly dominant at higher redshifts, while the fraction of bright early–type galaxies decreases. To follow the same galaxy population at different redshifts we therefore correct for evolution using a luminosity–selected, volume–limited sample with a cut–off which evolves with luminosity. In particular, to track the evolution of the morphology–density relation over the redshift range $0.2 \leq z < 1$ we select objects with $M_{B_{AB}} < -20.5-z$ as these galaxies are visible over the entire redshift range.

The redshift evolution of the morphological mix in different environments is shown in Figure 8 for evolving–luminosity (upper panels) and stellar–mass selected (lower panels), volume–limited samples. Figure 9 instead shows the growth rate for early-type, spiral and irregular galaxies as a function of the environment.

The upper panels of Figure 8 show that in the redshift range $0.2 \leq z < 1$ the evolution of the relative fraction of early–type, spiral and irregular galaxies depends on the environment. Little evolution is seen in the early–type population in low density environments, while we see a monotonic rise with cosmic time in the highest density regions. We can confirm with our data the behaviour found by Smith et al. (2005) at intermediate densities, where the evolution seems to occur quite recently with little evidence for any change at earlier epochs. When focusing on spiral galaxies, the lack of evolution at intermediate and high density regions is striking. Some degree of evolution in the fraction of spiral galaxies is instead visible in low density environments. To counterweight the evolution observed in the early–type population we expect a strongly evolving trend for irregulars, that is in fact what is found. Figure 8 finally confirms that the relative fraction of morphological types changes with redshift and environment.

Galaxy luminosities are very sensitive to bursts of star formation, which are frequent at the high redshifts considered. Since stellar masses are expected to change less rapidly with redshift, we opt for the use of mass–selected samples. In doing that, we simply cut the luminosity–selected, volume–limited samples at $10^{10.8}$ $M_{\odot}$. The results are shown in the second row of Figure 8. The trends we observe for this sample are extremely different from the ones seen for the luminosity–selected, volume–limited sample. Irregular galaxies are not plotted here due to their very small number at such high stellar masses. In the lowest and inter-

mediate density environments we witness a trend consistent with lack of evolution for both early–type and spiral galaxies. Some indications of evolution, although at low statistical significance, less than the 2σ level, is present in the densest regions. As already shown in Section 2.3 and Figure 3 the main difference between the evolving–luminosity and the stellar–mass selected samples is in the presence in the first sample of low mass, star forming galaxies which are not included in the mass–selected sample. This suggests that these objects as the main responsibles of the evolution seen in the luminosity volume–limited samples.

We define the growth rate of the fraction of a specific morphological type in a given environment as the best fit slope of the morphological mix evolutionary trends shown in Figure 8. The timing of environmental evolution of the galaxies morphological mix can be investigated just looking at Figure 9, where the growth rate for each morphological type considered in this study is shown as a function of the environment. In Figure 9 we plot the absolute value of the best fit slope, which can be taken as a measure of the efficiency of the morphological evolution. For luminosity volume–limited galaxy samples, strong evolution is seen in low density environments for spirals and irregulars, in contrast to the small evolution of early–type galaxies. The trend is clearly inverted in denser environments. In the case of mass–selected samples, almost no evolution is seen independently of the environment and/or of the morphological type, with the possible exception only in the highest density environment.

Our results are based on the assumption that the luminosity evolution is the same for all galaxies independently of their morphology, which might not be the case. As control check we therefore define evolving absolute magnitude cuts, different for each of the 3 morphological classes considered, and we follow the redshift evolution of the relative population in different environments. To parametrise the evolution we use the values of M^* obtained in Zucca et al. (2009) in a B rest–frame band with $h = 0.7$ and with a fixed α defined in the redshift range $0.3 < z < 0.8$. The evolution of M^* is then fitted with a simple linear function for each morphological type. Despite the fact that the value of M^* varies as a function of the galaxy morphological type we observe that the final general trend does not change, confirming that the result is robust and does not strongly depend on the specific value assumed for the luminosity evolution.

5. Morphological mix of red and blue galaxies

In this section we further explore the contribution of different stellar populations to the morphology–density relation in order to disentangle dynamical and star formation history contributions and better study the relative importance of the environment and of the physical mechanisms which determine galaxy stellar masses to the galaxy segregation.

The galaxy morphology could be viewed as the end result of its dynamical history. Frequent high speed galaxy encounters (galaxy harassment) drive the morphological transformation of galaxies in clusters, leading to dramatic evolution of disk galaxies (Lake et al. 1998). Ram pressure stripping and tidal stripping also play a key role in transforming galaxies in clusters centres. In our survey we do not sample such rich clusters, which are rare such that galaxies in this environments represent only 1% of the population at z ∼ 0. Galaxy mergers are believed to be the primary mechanism that creates ellipticals, if the merger involves two spiral galaxies that have approximately the same mass (i.e. major merger) and happens in a way that drives away much of the dust and gas through a variety of feedback mechanisms.

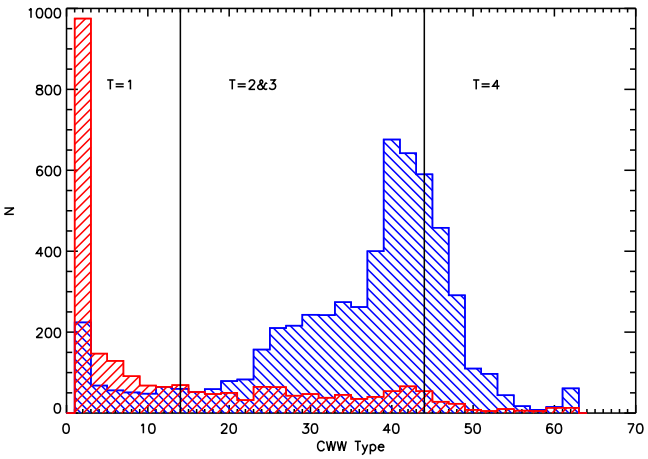

Fig. 10. Distribution of the extended CWW templates as a function of the morphological type. The early–type distribution is represented by the red (45°–inclined) shaded histogram, while the late–type population is shown by the blue (−45°–inclined) shaded histogram. Vertical lines separate the spectrophotometric types: T=1,2,3,4 corresponds to E/S0, early spiral, late spiral and irregular/starburst templates, respectively.

By definition, galaxies spectrophotometric types depend on galaxy colours, which themselves depend on the recent star formation. To assign our galaxies to spectrophotometric classes, we have fitted their observed multi–band photometry with the spectral energy distribution of sixty–two CWW (Coleman et al. 1980) extended templates plus two starburst templates (Kinney et al. 1996). Galaxies are then divided into four spectrophotometric types, according to their spectral energy distribution from UV to near–IR, corresponding to E/S0 (type 1), early spiral (type 2), late spiral (type 3) and irregular (type 4) templates. The two starburst templates are included in type 4. As shown in Zucca et al. (2006) going from type 1 to type 4 objects the composite spectra have a bluer continuum with increasingly stronger emission lines.

The existence of high–resolution HST/ACS imaging and multi–wavelength coverage of the COSMOS field allows to combine and compare morphological and spectrophotometric information. We name early–type galaxies with a spectrophotometric type 2, 3 or 4 ($CWW \geq 14$) "blue", while the ones with spectrophotometric type 1 are named "very red" when fitted by the most extreme type 1 template ($CWW = 1$) and "red" when fitted by the other type 1 templates ($2 \leq CWW < 14$). The same logic is used to classify late–type objects in a "red" population, when fitted by type 1 templates ($1 \leq CWW < 14$), in a "blue" population, when the spiral templates of type 2 and 3 ($14 \leq CWW < 44$) are the best fit of the galaxy SED and in a "very blue" population when fitted by the more extreme starburst templates ($CWW \geq 44$) corresponding to type 4.

Figure 10 shows the distribution of early and late–type galaxies as a function of the spectrophotometric templates. The 45° inclined red shaded histogram represents the morphological early–type galaxies, while the −45° inclined blue shaded one represents the late–type galaxies in our sample. We observe a tail in the histogram of early–type galaxies extending bluewards, up to the irregular and starburst spectrophotometric templates. A visual check of these objects reveal that ∼ 37% of them are face–on late–type galaxies with morphological parameters typical of an early–type population (for more details, see Cassata et al., in

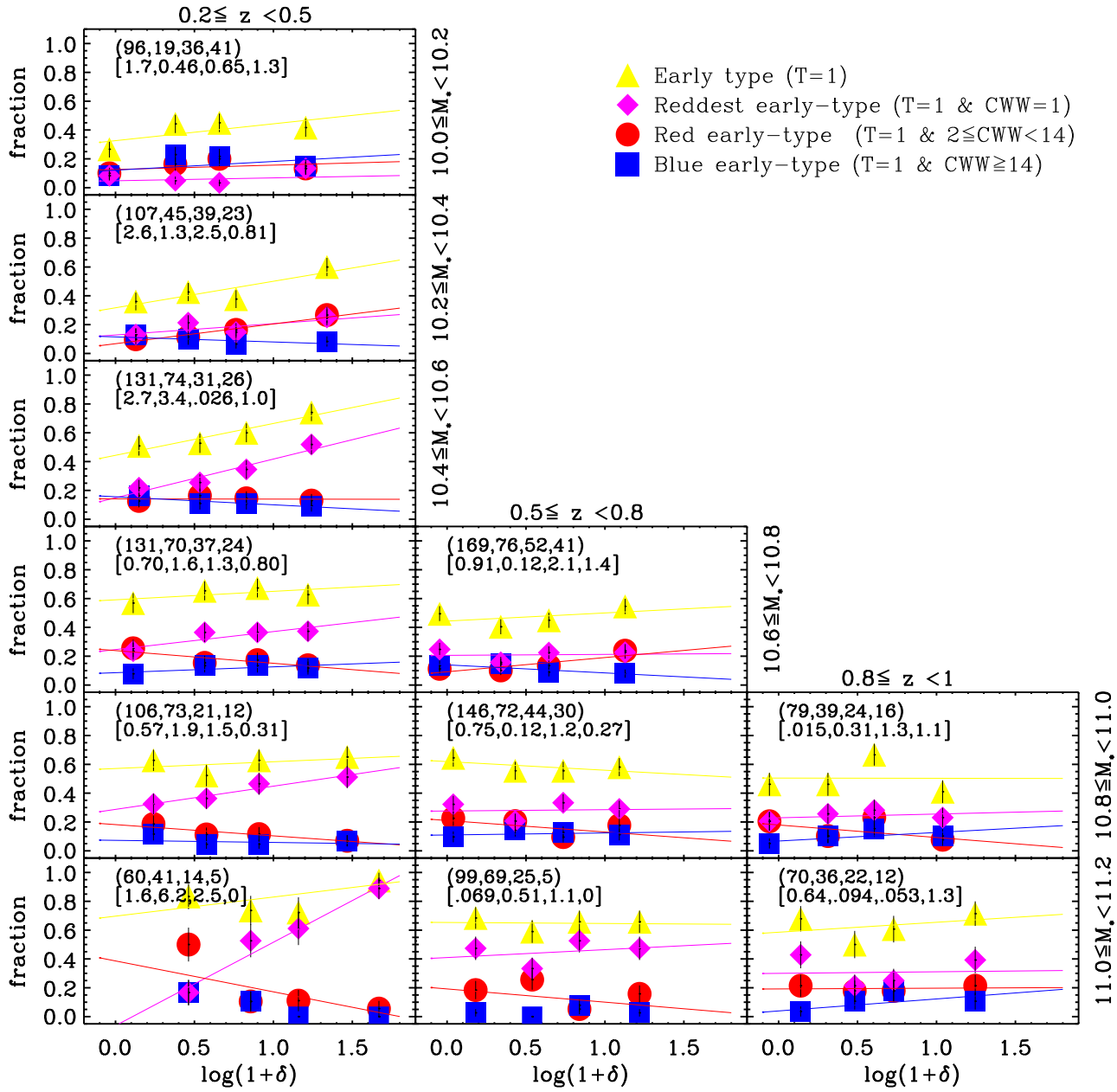

Fig. 11. Contribution of the various spectrophotometric types to the early–type population in different environments. The percentage of the whole morphologically classified early–type population, as well as the percentage of the spectral type subclasses, is plotted as a function of the mass–weighted galaxy overdensity computed using the 5^{th} nearest neighbour density estimator with volume–limited tracers. The redshift increases from the left to the right (as indicated on the top), while objects are progressively more massive from top to bottom (as indicated on the right–end side). The entire early–type population is represented with filled yellow triangles. This population is then divided into 3 subclasses according to the galaxy spectral type: filled magenta diamonds correspond to very red spectral type ($CWW = 1$); filled red circles represent E/S0 fitted by the templates 2–13; blue early–types ($CWW \geq 14$) are represented with blue filled squares. Enclosed in parenthesis are the total number of galaxies in the stellar mass and redshift bin considered, as well as the number of very red, red and blue early–type objects. Within square brackets we give the significance of the deviation from zero of the slope of the linear fit.

preparation). The existence of a dominant bulge and the consequent small contribution of the disk component in the estimation of the structural parameters used in the automatic galaxy classification procedure is one of the reasons that we bring forward to

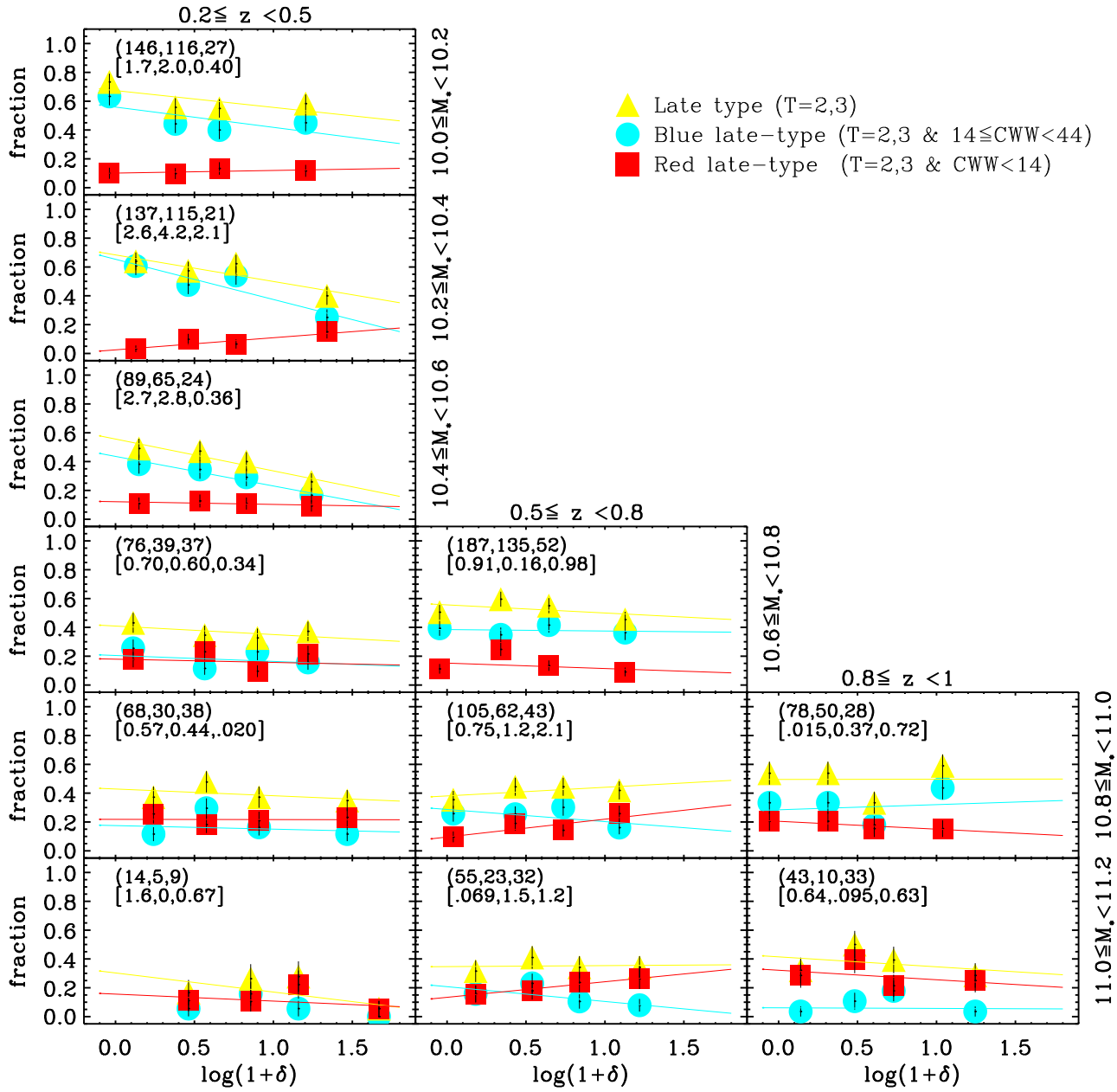

Fig. 12. Contribution of the various spectrophotometric types to the late–type population in different environments. The percentage of the whole morphologically classified late–type population, as well as the percentage of the spectral type subclasses, is plotted as a function of the mass–weighted galaxy overdensity computed using the 5^{th} nearest neighbour density estimator with volume–limited tracers. The redshift increases from the left to the right (as indicated on the top) while objects are progressively more massive from top to bottom (as indicated on the right). The entire late–type population is represented with filled yellow triangles. This population is then divided into 2 subclasses according to the galaxy spectral type: filled cyan circles represent early and late spirals fitted by the templates 14–43; red late–types ($CWW \leq 13$) are represented with red filled squares. Irregular and starburst spectral types ($CWW > 43$) are not shown, since they are not present at the masses considered. Enclosed in parenthesis are the total number of objects in the mass and redshift bin considered, as well as the number of blue and red late–type objects. Within square brackets we give the significance of the deviation from zero of the slope of the linear fit.

explain why those objects are automatically classified as early–type. In order to explore more in detail this population, stacked spectra have been produced following Mignoli et al. (2009). The composite spectra of "blue" early–types present prominent emis-

sion lines (Zucca et al. 2009): low mass "blue" early–type galaxies have stacked spectra, typical of star forming galaxies, with blue continuum and emission lines; the composite spectra of more massive "blue" early–types galaxies show emission lines on top of a red spectra with absorption lines. For massive "blue" early–type galaxies, the presence of a central AGN could explain the high concentration we measured for these galaxies on HST/ACS images. Evidence for blue colours or star formation signatures in the spectra of early–type galaxies has been reported by various studies in the past (Schade et al. 1999; Im et al. 2001; Menanteau et al. 2001, 2004; Cross et al. 2004; Cassata et al. 2005; Treu et al. 2005a; Cassata et al. 2007). The latter paper in particular studied in detail the properties of the blue early–type population in a sub–set of the COSMOS ACS data centered around z $\sim$ 0.7, showing in particular that their fraction is independent of local density.

We note that $\sim$ 13% of late–type galaxies populate the tail of the histogram extending redwards. Furthermore, we note that the peak corresponding to the reddest template ($CWW = 1$) contains a considerable fraction ($\sim$ 16%) of extremely red late–type galaxies. We decided to visually inspect all the morphologically late–type objects with a SED better fitted by a red template to be reassured that our population of red late–type galaxies is real and not simply due to an error in the morphological classification. We find in this class of objects a well characterised population of edge–on spiral galaxies, often dominated by a strong dust line and therefore highly reddened. This is in agreement with what already found in the DEEP survey by Weiner at al. (2005), in the GEMS survey by Bell et al. (2004b) and in the COSMOS field by Cassata et al. (2007). The latter paper in particular is based on a subset of the same ACS observations used here and discusses in detail how this population of highly–inclined dust–reddened spirals represents a $\sim$ 30% contamination in a colour–selected sample of supposedly passive red galaxies.

Once this careful check performed, we create the "clean" and "complete" samples, used in our analysis and introduced in Section 3.1. They are defined in this way: the "clean" sample is the one for which blue ellipticals are removed from the morphologically classified early–type population, the spiral class staying unchanged; instead in the "complete" sample the blue ellipticals are added to the morphologically identified spiral galaxies.

6. colour dependence of the morphology–density relation

If we allow for the existence of an environmental dependence of the global stellar mass function (Bolzonella et al. 2009) and of strong mass–morphology, mass–density and mass–M/L relations, the morphology–density relation at constant luminosity could be interpreted as due to selection effects. We therefore consider only stellar–mass selected, volume–limited samples to investigate the role of the star formation history on the morphology–density relation. We start our investigation from the morphology–density relation shown in Figure 7 and we combine morphological and spectrophotometric information.

In Figure 11 we show the contribution of different spectrophotometric types to the early–type population, going from sparse to high density regions, as a function of galaxy stellar mass. The blue early–type galaxies show a behaviour with respect to the density either consistent with being flat or decreasing with density, typical of a late–type population, even if always at less than 2σ significance. This is expected since, as mentioned above, this population is largely composed by face–on, bulge–dominated spirals. We now compare the relative contribution of very red and red early–type galaxies to the slope of the morphology–density relation in different stellar mass and redshift bins. We observe that at z $<$ 0.5 and for all the stellar mass bins considered, the morphology–density relation for the very red galaxies (magenta diamonds) is present at few σ level, while the contribution of the other spectrophotometric types to the global trend (yellow triangles) is pretty negligible and consistent with being flat.

In Figure 12 we show the contribution of different spectrophotometric types to the morphology–density relation of the late–type population as a function of galaxy stellar mass. The contribution of starbursts and irregulars becomes negligible at the considered stellar masses and it is therefore not shown. The panels of Figure 12 show how the population of red late–type galaxies, that is in part produced by the spurious effect of internal reddening, is substantially independent of local density (apart from local fluctuations due to small number statistics as in the lowest–redshift, lowest–mass bin). This is expected, as it only depends on the galaxy inclination with respect to the line–of–sight (see also Cassata et al. (2007) for a direct measurement of the dependence of colour on galaxy inclination). Thus, the overall late–type population is intrinsically described by blue templates only. These fully drive the observed lack of dependence on local density for massive galaxies and the limited dependence at small masses and low redshift. The comparison in each single panel of Figure 12 of the significance of the slope of the linear fit of the morphology–density relation for different spectrophotometric types shows that either no morphology–density relation is present for red late–type objects (red squares) or that this population has a preference for high density regions, like early–type galaxies. The spiral spectrophotometric types (cyan dots) are responsible for the observed late–type galaxy segregation at masses smaller than $10^{10.6}$ $M_{\odot}$.

The interpretation of Figure 11 and 12, where we investigate how the star formation history affects the morphology–density relation as a function of galaxy stellar mass, could be done in terms of the aging of the stellar population. We already claimed from Figure 7 that there is no morphological segregation, in the galaxy population as a whole, at least for masses larger than $10^{10.6}$ $M_{\odot}$ at any redshift. In Figure 11 we observe that at z $<$ 0.5 and at fixed mass, within the unsegregated early–type population, there is a systematic colour/age segregation: redder and therefore older galaxies (magenta diamonds) show a stronger dependence on the environment than the younger population (red dots). This behaviour seems to soften at higher redshifts, where the dependence on the environment of the spectrophotometric types (of which the early–type population is the global representation) is consistent with being flat. An age dependence on the environment is also visible in Figure 12, where blue and red spirals often present an opposite trend with environment. In the Sloan Digital Sky Survey (SDSS) (Blanton et al. 2005; Quintero et al. 2006) and more recently in the GalaxyZoo project (Bamford et al. 2009) it is found that galaxy colour is more strongly correlated with environment than morphology and that colour and morphology bimodalities are largely independent functions of environment. Our results show the same but, for the first time, at high redshift. This result, combined with the lack of morphological segregation for high mass galaxies, is an indication that morphology is a galaxy scale property while star formation is more affected by large scale structure.

7. Discussion

A strong consequence of the cold dark matter paradigm in cosmology is the hierarchical scenario of galaxy formation according to which haloes are assembled from smaller units through mergers. A number of studies confirm that galaxies, located in these dark matter haloes, are complex systems and their evolution definitely depends on the interplay of various factors such as star formation history, chemical enrichment, feedback and dynamical effects, including mergers. All these parameters have their importance, at different times in the life of a galaxy, in shaping the great variety of objects we observe.

In addition to this work, a set of related studies, also based on zCOSMOS spectroscopy and COSMOS photometry, approach this topic using a variety of statistical tools (Bolzonella et al. 2009; Pozzetti et al. 2009; Zucca et al. 2009) and analysis (Cucciati et al. 2009; Kovač et al. 2009; Iovino et al. 2009) to understand how star forming history, stellar mass, environment and merger history (de Ravel et al. 2009b; Kampczyk et al. 2009; Tresse et al. 2009) differently act to determine the properties of individual galaxies.

7.1. Comparison to previous studies

Significant progress has been made in the understanding of the environment–morphology connection since Dressler et al. (1980) first claimed that a relation exists between the morphology of a galaxy and the environment in which it resides. A quantitative comparison of our results with previous analyses is not straightforward mainly because of the different morphological classification schemes and density estimators adopted in the various surveys. Compared to many previous studies, we have the advantage to use a surface density estimator (number of galaxies in cylinder divided by the circular area, but with the real distances) which properly corrects for all the survey observational biases (Kovač et al. 2009). We also fully exploit the possibility of accurate morphological classification over an unprecedented volume provided by the COSMOS HST/ACS imaging (Scoville et al. 2007; Koekemoer et al. 2007), building upon previous morphological analyses of the same data set (Capak et al. 2007; Cassata et al. 2007; Guzzo et al. 2007).

Cooper et al. (2005) claim that environmental investigations require good precision spectral measurements to reconstruct the galaxy distribution down to small scales. The early environmental analyses of the COSMOS data presented in Capak et al. (2007), Cassata et al. (2007) and Guzzo et al. (2007) show that spectroscopic redshifts are needed to recover density/structures in low density environments, which is where a large fraction of galaxies live. However, in high density regions the environment can be properly recovered using high quality photometric redshifts. Large and deep redshift surveys are therefore the best probes of the density field delineated by galaxies at all redshifts since they definitely increase the dynamic range of density which can be recovered. In this respect, the zCOSMOS survey was designed to reconstruct the 3D density field out to $z \sim 1$, from 100 kpc to 100 Mpc scale, with much better resolution in the radial direction than it has been possible with photometric redshifts or weak lensing.

The main observational obstacle in probing the structure of high redshift galaxies is the seeing–limited and limited spatial resolution of ground–based images which can introduce significant classification biases, ie. galaxy structures such as spiral arms and tidal tails get progressively smoothed out with increasing redshift. Among the large number of quantitative classifiers that have been developed or extended over the years we opt in this study for an innovative non–parametric approach (see Section 3.1 for more details) which allows for a uniform classification up to $z \sim 1$.

Galaxy spectrophotometric types are often used instead of morphological types since they can be measured directly from multi–wavelength photometry. In addition, the results interpretation is strictly related to colour studies and benefits of interesting literature (Cooper et al. 2006; Cucciati et al. 2006). However, we clearly observed that morphological and spectral types do not fully overlap and complementary information are obtained when using both of approaches, as in this work. colour studies are more related to the galaxy stellar population and its star formation history, while morphological studies tell us more about the effects of dynamics and environment on galaxy evolution.

Recent relevant works (Smith et al. 2005; Capak et al. 2007; Guzzo et al. 2007; Van der Wel et al. 2007) look at the effects of the environment on morphological evolution up to $z \sim 1.2$. In many of these studies the environment is computed following the method first introduced by Dressler et al. (1980) and often adopted later on (Dressler et al. 1997; Postman et al. 2005). The projected number density is calculated by counting the 10 nearest neighbors and dividing by the rectangular area enclosed enclosed by them. Contamination from the projection of field galaxies at lower and higher redshifts is corrected in Smith et al. (2005) using Postman et al.'s (1998) I–band number counts and in Capak et al. (2007) using photometric redshifts bins for the nearest neighbor counting. Van der Wel et al. (2007) also used local projected surface densities, but measuring the distance to the nth nearest neighbor more massive than $4x10^{10}M_{\odot}$ to be more consistent with their choice to work with mass selected samples. The morphological classification instead is quite inhomogeneous in its definition through the various studies and sometimes within the same study. An exception is the work by Capak et al. (2007), who introduce the use of the Gini coefficient measured in a Petrosian aperture as a stand alone parameter able to clearly separate early and late type galaxies with $0.3 < z < 1.2$ using the ACS F814W filter. Smith et al. (2005) visually classified 1257 galaxies in high density clusters and low density fields starting from HST/ACS observations at $z \sim 1$. To discern evolutionary trends they compare with Dressler (1980) at $z \simeq 0$ and with Dressler et al. (1997) and Treu et al. (2003) at $z \simeq 0.5$. van der Wel et al. (2007) automatically classified their sample of more than 2000 galaxies using the Sérsic parameter n and a measure of the residual (B) from the model fit (Blakeslee et al. 2006). They claim that their morphological classification of galaxies has been quantified in an internally consistent manner both in the local universe and at high redshift and that the $n - B$ classification is the condition to achieve this result. The reason is that they take into account the PSF smearing effect and this is essential when a sample with very different photometric properties is used to study redshift dependent trends.

In their study on the COSMOS field, Guzzo et al. (2007) found that at z=0.73 the morphology–density relation was already in place with a globally lower fraction of early–type galaxies ($\sim$ 65%) than at z=0 for comparable local densities, while Capak et al. (2007) conclude that galaxies are transformed from late to early type more rapidly in dense than in sparse regions and that no evolution at all is found at $z > 0.4$ at densities below 100 galaxies Mpc^{-2}. Their findings are qualitatively in agreement with Smith et al. (2005) who show that the early type fraction is $\sim$ 3 times steeper locally than at z=1 and that most of the evolution responsible of the observed local trend occurred at $z < 0.5$. Van der Wel et al. (2007) opt for an innovative approach

and get as main result that the fraction of early type galaxies more massive than $4 \times 10^{10} M_{\odot}$ in the field and group environment has remained constant since $z \sim 0.8$ and that therefore the galaxies evolution in mass, morphology and density should happen without changes in the morphology–density relation.

Where overlapping, our results are in agreement with previous works on the evolution of the morphology–density relation and possible small differences can be explained by the involved approach. Nonetheless it should be stressed that the strength of our results is additionally supported by the homogeneity of the sample used for the analysis. Using luminosity and stellar mass volume limited samples, splitted in five redshift intervals up to $z\sim 1$, we looked at information on morphological evolution rates for galaxies above some limiting luminosity or stellar mass. We additionally looked at the difference between colour and morphology–density relation. Previous studies have the merit for already exploring the behaviour of certain galaxy properties in well defined environments, often clusters, and in specific luminosity, mass and redshift ranges But it is the first time that a comprehensive analysis is done using a complete, well-checked and uniform set of spectroscopic and photometric data. For this unique characteristic of our data, the scenario they describe allow to tie together previous findings in a simple general view.

7.2. Role of the environment on galaxy formation and evolution

How do galaxies form and what determine their evolution? Is the destiny of a galaxy established by birth or are external factors important? Which is the role of the environment in the complex scenario we can put together using the large number of observational and theoretical analyses carried out in the last decades? Is the morphology–density relation an intrinsic galaxy property, "nature" hypothesis, or is due to the environment, "nurture" hypothesis?

From an observational point of view, the downsizing in galaxy formation (Cowie et al. 1996; Gavazzi et al. 1996) predicts that more massive galaxies cease to form stars at early epochs, while less massive systems stay active longer. This apparent anti–hierarchical scenario is also supported by other studies in the local universe (e.g. Kauffmann et al. 2003) and at high redshift (e.g. Glazebrook et al. 2004). In addition, Juneau et al. (2005) show that the more massive galaxies start to form stars earlier than intermediate and low mass objects. More massive galaxies also acquire galactic structures like bars earlier, showing that dynamical maturity of disks also follows cosmic downsizing (Sheth et al. 2008). Finally, Einasto et al. (2005) claim that clusters in high density regions evolve more rapidly than in low density environments, supporting the theoretical expectation of an acceleration of structure formation in denser environments.

From a theoretical perspective, Frenk et al. (1985) performed the first numerical simulation of a flat CDM universe and claimed that the assumed hierarchical clustering model is consistent with the observed dynamics of galaxy clustering only if galaxy formation is biased towards high density regions. Therefore, they first proposed that the morphology–density relation is a natural consequence of a hierarchical scenario of galaxy formation. As shown, among others, by Frisch et al. (1995), the first objects to form in simulations are rich clusters in superclusters. More recently, high–resolution simulations and semi–analytic models of galaxy formation (de Lucia et al. 2006) confirm the trends of deep high redshift surveys.

Because of the properties of our data, the following considerations on the mechanisms involved in the formation and evolution of galaxies are focused on the history of massive galaxies from $z \sim 1$ to present. We start from a scenario, supported by numerical simulations and ultra deep observations, in which the early universe is mainly populated by spirals and irregulars. Various studies claimed that massive early type galaxies are already in place at z=1. De Ravel et al. (2008), using VVDS data, show that major mergers account for about 20% of the mass assembled in present day galaxies with masses $> 10^{10}$ solar masses, the rest being due to minor mergers and passive evolution. Early type galaxies should therefore form either by environmental effects such as merging and interaction, or simply by stopping star formation after losing or exhausting their gas. Moreover some early type galaxies may have formed since the beginning as ellipticals and not from the transformation of spirals and irregulars.

Intuitively, the most massive galaxies at any epoch should be the final product of the evolutionary chain: either they assemble very fast by mergers or they form very early.

We already discussed that the evolutionary scenario we can deduce from the study of the morphology–density relation in luminosity–selected samples may be largely a consequence of the biased view imposed by our B–band luminosity selection. Nonetheless, we explored the results of this approach for comparison to previous works which adopted the same luminosity selection. The stellar–mass selection is instead a more physical approach on the basis of which to identify the key players in galaxy evolution.

From our analysis we observe that when considering a luminosity volume–limited sample, the fraction of early type galaxies changes as a function of the environment up to $z \sim 1$: in high density regions we observe a larger fraction of early type objects compared to low density environments (see Figures 5 and 8). We interpret the observed morphological segregation as the combined result of the existence of an environmental dependence of the global stellar mass function (Bolzonella et al. 2009) and of the well–known mass–morphology and mass–M/L relations.

The volume–limited, stellar–mass selected sample used in this study allows considerations on the evolution of galaxies more massive than $10^{10.6} M_{\odot}$ and on the role of less massive objects. The existence of a critical mass above which we do not observe any morphological dependence with respect to the environment (see Figure 7) suggests that, at least for what concerns massive galaxies, the intrinsic mechanisms of galaxy formation might be more fundamental than the environmental processes. In addition, the comparison of the flat slope of the morphology density relation seen in a stellar–mass volume–limited sample with the trends existing when using a luminosity volume–limited sample brings to the conclusion that blue galaxies less massive than $10^{10.6} M_{\odot}$, for which our B–band luminosity selection misses the red counterparts, are likely to be the main contributors to the evolution observed in the luminosity volume–limited sample.

Which scenarios could be advocated to speculate on the causes of the surviving of a morphology–density relation at masses lower than $10^{10.6} M_{\odot}$ and for the existence of the differences in the galaxy stellar mass function for low and high density environments? We consider the following alternatives:

– starting from a uniform distribution of galaxies, there has been a more effective transformation in high than in low density environments. The "nurture" scenario is preferred.

– since the beginning there are more ellipticals in denser regions. If "nature" acts alone, the fraction of early type galaxies should stay mostly constant with time. We should therefore combine this hypothesis with the one that the highest density regions are the first to collapse and have consequently more time to increase their early type population by merging and environmental effects.

The environment also affects the growth morphological populations: the early–type fraction increases faster in dense than in sparse regions, the opposite happening for spirals. Within the limits of our statistics, irregulars seem not to feel the environment, they strongly evolve in redshift regardless of the environment (see Figure 9). These results point towards an environmental dependence of the different processes governing galaxy formation, which can preferentially act on high or low density regions.

Another ingredient which contributes to the general picture and that we can extrapolate from our data is that morphology and star formation appear to be affected by different processes. We show that at high galaxy stellar masses morphology is not driven by the environment, while galaxy colours are still affected by it (see Figure 11). Is the growth in the early type fraction mainly driven by interactions, while the reduction in star formation is caused by gas stripping?

We conclude that both "nature" and "nurture" play, at different epoch in the history of a galaxy, an important role in shaping the large variety of objects we observe in the local universe as final result of the evolutionary chain.

8. Summary & conclusions

We use the so–called 10k sample, constituted by the first 10644 observed galaxies with spectroscopic redshifts of the "bright" zCOSMOS survey, to study the evolution of the morphology–density relation up to $z \sim 1$ for luminosity and stellar mass selected, volume–limited galaxy samples. We use the density estimates of Kovač et al. (2009) who introduce a new algorithm, implemented in the ZADE code (Kovač et al., 2009), to derive the 3D density field. This new algorithm makes advantage of the high sampling rate of our spectroscopic sample as well as of the high accuracy of the photometric redshifts measured in the COSMOS field. The high resolution and depth of the HST/ACS imaging available in the field is essential to perform an objective, automatic and unbiased morphological classification. It is the first time that the morphological mix can be split into early type, spiral and irregular galaxies up to $z \sim 1$ for such a large sample. Finally, the unique multi–λ coverage of the COSMOS field is essential for an accurate estimate of galaxy stellar masses and spectrophotometric types. The COSMOS and zCOSMOS surveys are therefore the first surveys to enable the study up to $z \sim 1$ of the impact of the environment on galaxy formation and evolution, trying to disentangle nature and nurture effects, using a complete and homogeneous sample with high quality control in spectral measurements.

In agreement with previous studies (Postman et al. 2005; Smith et al. 2005; Capak et al. 2007) we see that the morphology–density relation, in luminosity selected volume–limited samples, was already in place at z=1, but tends to be flatter than at lower redshift. This is also in agreement with the observed trends in the colour–density relation (Cooper et al. 2006; Cucciati et al. 2006). In addition, we observe a luminosity dependence of the morphology–density relation: the morphological segregation is stronger for the brightest galaxies at each redshift. Nonetheless, at least at the lowest redshifts considered for our analysis, the environment acts more effectively on low luminosity early–type galaxies, affecting more their star formation and morphology in dense regions. This behaviour is reversed for late–type objects suggesting a different role of the environment on the morphological mix at the same luminosity. Looking at the dependence with respect to the local overdensity of the spectrophotometric types relative to the early–type population we conclude that the brightest and reddest galaxies at each redshift are responsible of the global trend observed.

zCOSMOS enables us to investigate whether the strong effects we are witnessing in luminosity selected volume–limited samples are simply due to a biased view induced by the B–band luminosity selection or a more fundamental relation among galaxy stellar masses, environment and morphology does also exist. In fact, the morphology–density relation observed in the luminosity–selected sample can be considered as a "selection effect" arising from the existence of an environmental dependence of the galaxy stellar mass function (Bolzonella et al. 2009) and the well–known mass–morphology and mass–M/L relations. We additionally observe, when using luminosity–selected, volume–limited samples, a strong environmental dependence in the evolution of early–type and spiral galaxies in the explored redshift range: the behaviour of the early–type population with redshift is consistent with no evolution in low density regions, while showing a monotonic increase with cosmic time at intermediate and high overdensities; the evolution with redshift of spiral galaxies as a function of the environment has the opposite trend with respect to early–type galaxies. In contrast irregulars seem to strongly evolve regardless of the local environment.

When considering stellar–mass selected, volume–limited samples the aforementioned trends are much less significant, supporting the hypothesis that the observed evolution is due to low mass, bright, star forming galaxies for which the B–band luminosity selection misses the equally low mass red counterparts.

We stress the importance of using a stellar–mass selected, volume sample in order to obtain an information less biased by the galaxy star formation history and more physical. Is there a critical mass which separates galaxies into two families having a different behaviour with respect to the environment? Is the galaxy stellar mass or the environment the primary driver of the morphological differentiation? Is the mass a more fundamental parameter than the environment in which a galaxy lives? Our data show that at masses lower than $10^{10.6} M_{\odot}$ the morphology–density relation is present at $\sim 3\sigma$ level. At higher stellar masses we witness a change in this behaviour, with galaxies of a specific morphological type not showing any environment dependence. Since galaxy stellar mass is the result of several processes, including conditions at birth, this result seems to indicate that the physical processes that determine the morphology of massive galaxies are rather independent of the environment or that at least at $z < 1$ massive galaxies evolve independently of the environment.

Interestingly we still observe a colour segregation for a specific morphological type in mass regimes where no morphology–density relation can be claimed. We then conclude that there is a colour dependence on the environment beyond that on morphology up to $z \sim 0.5$, with some hints at higher redshifts, most likely related to environment dependent star formation histories.

Even if the zCOSMSOS 10k sample allowed for a great improvement and refinement in our understanding of the role of the environment in shaping the Universe we observed, there are questions which are still without a precise answer mainly due to statistical limitation and to the limit in redshift imposed by

the relatively bright limiting magnitude. The 20k zCOSMOS "bright" sample, that we are finishing assembling, as well as higher redshift data from the zCOSMOS deep project should overtake these shortcomings and allow to extend our analysis to an epoch where important changes occur and to firmly establish the redshift at which the morphology density relation emerges.

Acknowledgements. LT acknowledge support from CNES. We thank CNES and PNC for support to the COSMOS project. This work has been partially supported by INAF grant PRIN-INAF 2007 and by the grant ASI/COFIS/WP3110I/026/07/0.

References

Abraham, R. G, van den Bergh, S., & Glazebrook, K. 1996, ApJS, 107, 1
Abraham, R. G, van den Bergh, S., & Nair, P. 2003, ApJ, 588, 218
Abraham, R. G., et al. 2007, ApJ, 669, 184
Arnouts, S., Cristiani, S., Moscardini, L., et al. 1999, MNRAS, 310, 540
Baldry, I. K., Balogh, M. L., Bower, R. G., Glazebrook, K., Nichol, R. C., Bamford, S. P., & Budavari, T. 2006, MNRAS, 373, 469
Bamford, S. P., et al. 2009, MNRAS, 393, 1324
Bell, E. F., et al. 2004, ApJ, 608, 752
Bershady, M. A., Jangren, A., & Conselice, C. J. 2000, AJ, 119, 2645
Blakeslee, J. P., et al. 2006, ApJ, 644, 30
Blanton, M. R., et al. 2003, ApJ, 594, 186
Blanton, M. R., Eisenstein, D., Hogg, D. W., Schlegel, D. J., & Brinkmann, J. 2005, ApJ, 629, 143
Brinchmann, J., et al. 1998, ApJ, 499, 112
Bruzual, G., & Charlot, S. 2003, MNRAS, 344, 1000
Bruzual, G., Charlot, S. 1993, ApJ, 405, 538
Bolzonella, O., et al. 2009, in preparation
Bottini, D., et al. 2005, Pub.Astr.Soc.Pac, 117, 996
Cowie, L. L., Songaila, A., Hu, E. M., & Cohen, J. G. 1996, AJ, 112, 839
Cassata, P., et al. 2005, MNRAS, 357, 903
Capak, P., et al. 2007, ApJS, 172, 99
Cassata, P., et al. 2007, ApJS, 172, 270
Cassata, P., et al. 2009, in preparation
Cimatti, A., et al. 2004, Nature, 430, 184
Coleman, G. D., Wu, C.-C., & Weedman, D. W. 1980, ApJS, 43, 393
Conselice, C. J., Bershady, M. A., & Jangren, A. 2000, ApJ, 529, 886
Conselice, C. J., Bershady, M. A., Dickinson, M., & Papovich, C. 2003, AJ, 126, 1183
Cooper, M. C., Newman, J. A., Madgwick, D. S., Gerke, B. F., Yan, R., & Davis, M. 2005, ApJ, 634, 833
Cooper, M. C., et al. 2006, MNRAS, 370, 198
Cross, N. J. G., et al. 2004, AJ, 128, 1990
Cucciati, O., et al. 2006, A&A, 458, 39
Cucciati, O., et al. 2009, in preparation
De Lucia, G., Springel, V., White, S. D. M., Croton, D., & Kauffmann, G. 2006, MNRAS, 366, 499
de Ravel, L., et al. 2008, arXiv:0807.2578
de Ravel, L., et al. 2009, in preparation
de Lucia, G. & Blaizot, J. 2007, MNRAS, 375, 2
De Lucia, G., Springel, V., White, S. D. M., Croton, D., & Kauffmann, G. 2006, MNRAS, 366, 499
Dressler, A., et al. 1997, ApJ, 490, 577
Dressler, A. 1980, ApJ, 236, 351
Einasto, J., Tago, E., Einasto, M., Saar, E., Suhhonenko, I., Heinämäki, P., Hütsi, G., & Tucker, D. L. 2005, A&A, 439, 45
Faber, S. M., & Jackson, R. E. 1976, ApJ, 204, 668
Frenk, C. S., White, S. D. M., Efstathiou, G., & Davis, M. 1985, Nature, 317, 595
Frenk, C. S., White, S. D. M., Davis, M., & Efstathiou, G. 1988, ApJ, 327, 507
Frisch, P., Einasto, J., Einasto, M., Freudling, W., Fricke, K. J., Gramann, M., Saar, V., & Toomet, O. 1995, A&A, 296, 611
Garilli, B., 2008, in preparation
Gavazzi, G., Pierini, D., & Boselli, A., 1996, A&A, 312, 397
Glasser, G. J 1962, J. Am. Stat. Assoc., 57, 648
Glazebrook, K., et al. 2004, Nature, 430, 181
Goto, T., Yamauchi, C., Fujita, Y., Okamura, S., Sekiguchi, M., Smail, I., Bernardi, M., & Gomez, P. L. 2003, MNRAS, 346, 601
Guzzo, L., et al. 1997, ApJ, 489, 37
Guzzo, L., et al. 2007, ApJS, 172, 254
Hogg, D. W., et al. 2003, ApJ, 585, L5
Holden, B. P., et al. 2007, ApJ, 670, 190
Huertas-Company, M., Rouan, D., Tasca, L. A. M, Soucail, G., & Le Fèvre, O. 2008, A&A, 478, 971
Ilbert, O., Tresse, L., Zucca, E., et al. 2005, å, 439, 863
Im, M., Faber, S. M., Gebhardt, K., Koo, D. C., Phillips, A. C., Schiavon, R. P., Simard, L., & Willmer, C. N. A. 2001, AJ, 122, 750
Iovino, A., et al. 2009, in preparation
Juneau, S., et al. 2005, ApJ, 619, L135
Kampczyk, P., et al. 2009, in preparation
Kauffmann, G., Nusser, A., & Steinmetz, M. 1997, MNRAS, 286, 795
Kauffmann, G., et al. 2003, MNRAS, 341, 54
Kauffmann, G., White, S. D. M., Heckman, T. M., Ménard, B., Brinchmann, J., Charlot, S., Tremonti, C., & Brinkmann, J. 2004, MNRAS, 353, 713
Kinney, A. L., Calzetti, D., Bohlin, R. C., McQuade, K., Storchi-Bergmann, T., & Schmitt, H. R. 1996, ApJ, 467, 38
Koekemoer, A. M., et al. 2007, ApJS, 172, 196
Kormendy, J. 1977, ApJ, 218, 333
Kovač, K. 2009, arXiv:0903.3409v1
Lake, G., Katz, N., & Moore, B. 1998, ApJ, 495, 152
Leauthaud, A., et al. 2007, ApJS, 172, 219
Le Fevre, O., Crampton, D., Lilly, S. J., Hammer, F., & Tresse, L. 1995, ApJ, 455, 60
Le Fèvre, O., Saisse, M., Mancini, D., et al. 2003, Proc. SPIE, 4841, 1670
Le Fèvre, O., Mellier, Y., McCracken, H. J., et al. 2004, å, 417, 839
Le Fèvre, O., Vettolani, G., Garilli, B., et al. 2005a, å, 439, 845
Lemson, G., & Kauffmann, G. 1999, MNRAS, 302, 111
Lilly, S. J., Le Fevre, O., Crampton, D., Hammer, F., & Tresse, L. 1995, ApJ, 455, 50
Lilly, S. J., Le Fevre, O., Hammer, F., & Crampton, D. 1996, ApJ, 460, L1
Lilly, S. J., Le Fèvre, O., Renzini, A., et al. 2007, ApJS, 172, 70
Lilly, S. J., et al. 2009, submitted
Lotz, J. M., Primack, J.,& Madau, P., et al. 2004, AJ, 128, 163
Menanteau, F., Ellis, R. S., Abraham, R. G., et al., 1999, MNRAS, 309, 208
Menanteau, F., Abraham, R. G., & Ellis, R. S., 2001, MNRAS, 322, 1
Mignoli, M., Zamorani, G., Scodeggio, M., et al. 2009, å, 493, 39
Menanteau, F., et al. 2004, ApJ, 612, 202
Mo, H. J., & White, S. D. M. 1996, MNRAS, 282, 347
Naim et al. 1995, MNRAS, 274, 1107
Nuijten, M. J. H. M., Simard, L., Gwyn, S., R&oumlttgering, H. J. A. 2005, ApJ, 626, L77
Oemler, A. J. 1974, ApJ, 194, 1
Papovich, C., Giavalisco, M., Dickinson, M., Conselice, C. J., & Ferguson, H. C. 2003, ApJ, 598, 827
, P., et al. 2009, in preparation
Petrosian, V. 1976, ApJ, 209, L1
Poggianti, B. M., et al. 2008, ApJ, 684, 888
Postman, M., & Geller, M. J. 1984, ApJ, 281, 95
Postman, M., & Lauer, T. R. 1995, ApJ, 440, 28
Postman, M., Lubin, L. M., & Oke, J. B. 1998, AJ, 116, 560
Postman, M., et al. 2005, ApJ, 623, 721
Pozzetti, L., et al. 2007, A&A, 474, 443
Pozzetti, L., et al. 2009, in preparation
Quintero, A. D., Berlind, A. A., Blanton, M., & Hogg, D. W. 2006, arXiv:astro-ph/0611361
Roberts, M. S., & Haynes, M. P. 1994, ARA&A, 32, 115
Scodeggio, M., Franzetti, P., Garilli, B., et al. 2005, PASP, 117, 1284
Schade, D., et al., 1999, ApJ, 525, 31
Scoville, N. Z., et al. 2007a, ApJS, 172, 1
Sheth, K., Regan, M. W., Scoville, N. Z., & Strubbe, L. E. 2003, ApJ, 592, L13
Sheth, K., Vogel, S. N., Regan, M. W., Thornley, M. D., & Teuben, P. J. 2005, ApJ, 632, 217
Sheth, K., et al. 2008, ApJ, 675, 1141
Smith, G. P., Treu, T., Ellis, R. S., Moran, S. M., & Dressler, A. 2005, ApJ, 620, 78
Taniguchi, Y., et al. 2007, ApJS, 172, 9
Tresse, O., et al. 2009, in preparation
Treu, T., Ellis, R. S., Kneib, J.-P., Dressler, A., Smail, I., Czoske, O., Oemler, A., & Natarajan, P. 2003, ApJ, 591, 53
Treu, T., et al., 2005a, ApJ, 622, L5
Tully, R. B., & Fisher, J. R. 1977, A&A, 54, 661
van der Wel, A., et al. 2007, ApJ, 670, 206
Weiner, B. J., et al. 2005, ApJ, 620, 595
White, S. D. M., & Rees, M. J. 1978, MNRAS, 183, 341
Windhorst, R. A., et al. 2002, ApJS, 143, 113
Wu, K. L.-K. 1999, Ph.D. Thesis,
Zucca, E., Ilbert, O., Bardelli, S., et al. 2006, å, 455, 879
Zucca, E., et al. 2009, in preparation

[1] Laboratoire d'Astrophysique de Marseille, CNRS-Univeristé d'Aix-Marseille, 38 rue Frederic Joliot Curie, 13388 Marseille Cedex 13, France
e-mail: lida.tasca@oamp.fr
[2] INAF-IASF, Via Bassini 15, I-20133, Milano, Italy
[3] INAF Osservatorio Astronomico di Brera, Via Brera 28, I-20121 Milano, Italy
[4] Institute of Astronomy, ETH Zurich, CH-8093, Zurich, Switzerland
[5] INAF Osservatorio Astronomico di Bologna, via Ranzani 1, I-40127, Bologna, Italy
[6] Department of Astronomy and Astrophysics, University of Toronto, 50 St. George Street, Toronto, ON M5S 3H4, Canada
[7] Dept. of Astronomy, University of Massachusetts at Amherst
[8] California Institute of Technology, MC 105-24, 1200 East California Boulevard, Pasadena, CA 91125 USA
[9] Spitzer Science Center, 314-6 Caltech, Pasadena, CA 91125, USA
[10] Laboratoire d'Astrophysique de Toulouse-Tarbes, Universite de Toulouse, CNRS, 14 avenue Edouard Belin, F-31400 Toulouse, France
[11] European Southern Observatory, Karl-Schwarzschild-Strasse 2, Garching, D-85748, Germany
[12] INAF - Osservatorio Astronomico di Padova, Padova, Italy
[13] Max-Planck-Institut für Extraterrestrische Physik, D-84571 Garching b. Muenchen, Germany
[14] Space Telescope Science Institute, 3700 San Martin Drive, Baltimore, MD 21218
[15] INAF Osservatorio Astronomico di Torino, Strada Osservatorio 20, I-10025 Pino Torinese, Torino, Italy
[16] Dipartimento di Astronomia, Universita di Bologna, via Ranzani 1, I-40127, Bologna, Italy
[17] Physics Division, MS 50 R5004, Lawrence Berkeley National Laboratory, 1 Cyclotron Rd., Berkeley, CA 94720, USA
[18] Centre de Physique Theorique, Marseille, Marseille, France
[19] Institut d'Astrophysique de Paris, UMR 7095 CNRS, Universite Pierre et Marie Curie, 98 bis Boulevard Arago, F-75014 Paris, France
[20] Universitäts-Sternwarte, Scheinerstrasse 1, Munich D-81679, Germany
[21] Argelander-Institut für Astronomie, Auf dem Hügel 71, D-53121 Bonn, Germany
[22] INAF, Osservatorio di Roma, Monteporzio Catone (RM), Italy